Motor Control of Heartbeat Coordination in the Medicinal Leech

By

Jason Kim

Emory University

Department of Neuroscience and Behavioral Biology

Ronald L. Calabrese, PhD.

Advisor

Katherine A. Boss-Williams, PhD.

Committee Member

Kristen Frenzel, PhD.

Committee Member

Astrid A. Prinz, PhD.

Committee Member

April 8, 2014

Motor Control of Heartbeat Coordination in the Medicinal Leech

By

Jason Kim

Ronald L. Calabrese, PhD.

Advisor

An abstract of
a thesis submitted to the Faculty of Emory College of Arts and Sciences
of Emory University in partial fulfillment
of the requirements of the degree of
Bachelor of Science with Honors

Program in Neuroscience and Behavioral Biology

2014

Abstract

Animals of the same species produce stereotyped motor patterns for movements such as breathing and heartbeat despite animal-to-animal variability in underlying neuronal networks and muscle performance. The Calabrese laboratory studies all aspects of the heartbeat system of the leech, from the central pattern generator (CPG) to the heart constrictions (Calabrese et al., 1995; Kristan et al., 2005). In the isolated nervous system, there is a large variability from animal-to-animal in the temporal and synaptic output of the CPG corresponding to similar variability in the fictive motor pattern (i.e. the motor pattern produced by the heart motor neurons in the isolated nervous system) (Norris et al., 2011). Despite this variability, the fictive motor patterns were all functional; they were recognizable as fictive heartbeats. Here we report studies on the variability of the heart constriction patterns in intact and semi-intact leeches as well as in a novel isolated ganglia chain-innervated heart, reduced preparation.

In the intact animal preparation, we use transparent leeches to visualize flow in the anterior segments. However, since such leeches are quite rare (<5%), only a select few produced analyzable video recordings (N=3). Optical recordings in semi-intact preparations were not possible due to loss of blood, so we measured the constriction pattern with a force transducer in multiple segments. We focused on the heart segments 8 and 12 in both semi-intact animals and reduced preparations recording bilaterally from force transducers. A custom MATLAB program quantifies the maximum rate of rise in constriction patterns of these heart segments across individual animals in the three different preparations. Our goal is to compare these constriction patterns with the motor patterns recorded *in vivo* (Wenning et al., 2014). Together, these experiments will help us understand whether variability in the constriction patterns and in the fictive motor pattern is similar.

Motor Control of Heartbeat Coordination in the Medicinal Leech

By

Jason Kim

Ronald L. Calabrese, PhD.

Advisor

A thesis submitted to the Faculty of Emory College of Arts and Sciences
of Emory University in partial fulfillment
of the requirements of the degree of
Bachelor of Science with Honors

Program in Neuroscience and Behavioral Biology

2014

Acknowledgements

Table of Contents

Table of Contents (cont.)

<u>Introduction</u>

Recent decades have focused the study of motor systems on the very building blocks of motor behavior: interactions between premotor and motor neurons in regulatory control of their functional motor outputs (Tresch et al., 2002; Rodriguez et al., 2012). Particularly in stereotyped movement, animals of the same species must produce similar stereotyped motor patterns for actions such as breathing and heartbeat, despite the intrinsic animal-to-animal variability in underlying neuronal networks (Goaillard et al., 2009). While selecting a particular motor behavior and investigating the underlying neurons and circuits involved is a valid method, this approach can only be optimally used in animals with well-identified, relatively simple nervous systems. These characteristics are true of many invertebrate nervous systems, making them ideal candidates for motor behavioral research.

The relation between the temporal pattern and synaptic strength profiles and the motor output have proven to be difficult to determine in vertebrate experiments because of the complexity of the spinal networks involved in their central pattern generator(CPG) systems. Some notable invertebrate studies have been conducted on the pedal ganglia of mollusks and their swimming behavior (Arshavsky et al., 1998) as well as the stomatogastric ganglion associated with chewing behavior in crustaceans (Prinz et al., 2003). Among other exceptional qualities, the medicinal leech in particular has a long history in these studies due to the readily manipulated and functionally unique properties of its nervous system (Kristan et al., 2005). The Calabrese laboratory specifically studies all aspects of the heartbeat system of the leech, from the control of motor behavior directed by the CPG to the heart constrictions in the tubular leech hearts. By using the more accessible heartbeat system of the leech, Norris, Wenning, Wright, and Calabrese (2011) showed that these intersegmental phase differences could be quantified by

measuring the functional output, or fictive heartbeat, of the heart excitor (HE) motor neuron bursts.

The core heartbeat CPG is comprised of seven identified heart interneuron (HN) pairs [HN(1)-HN(7)] and one unidentified pair of heart interneurons (Fig. 1). Five premotor pairs inhibit the 16 pairs of heart motor neurons which are tonic firers (Maranto and Calabrese, 1984). These neurons reside in the chain of ganglia, connected by a nerve cord (Fig. 2). The heartbeat CPG produces a bilaterally-alternating asymmetric pattern of activity of the premotor heart interneurons, which correspond in turn to an asymmetric fictive heart excitor (HE) motor pattern and an asymmetric constriction pattern of the two tubular hearts (Fig. 3), with regular switches in pattern between the two sides (Calabrese et al., 1995; Norris et al., 2011). The two observed premotor and subsequent motor patterns progress from rear (posterior) to front on one side and nearly simultaneously on the other, earning the names peristaltic and synchronous, respectively (Calabrese et al., 1995; Wenning et al., 2003; Wenning et al., 2004).

Interestingly, the motor pattern shows corresponding intersegmental coordination only from segment 15 upward. Further modeling and electrophysiological studies confirmed two additional pairs of heart interneurons located in the rear (Wenning et al., 2011). These produce a fictive motor pattern and the accompanying constriction pattern which progress from front to rear on both sides and converge in phase. Although they are still coordinated with the core heartbeat CPG, these new heart interneurons make strong inhibitory connections with the rearmost (segment 16 downward) heart motor neurons and contribute to a different motor and beating pattern in the rear (Wenning et al., 2011).

Subsequently, we were curious as to whether the previously undocumented anterior part of the animal also had similarly anomalous coordination compared to those observed in the

midbody segments. One focus of the present study is to record the heart activity in the anterior

portion of the animal, particularly in segments 2 and 3, and compare their phase relations to that

of their midbody counterparts. Trans-illuminated adult animals were video recorded *in situ*

across several beat cycles of peristalsis and synchronous to capture optical signal contrasts of

blood filling and emptying in the hearts.

We realize now that there is a large variation of intrinsic and synaptic parameters in

neuronal networks across animals, but the functional output of the networks is maintained within

individualized patterning (Goaillard et al., 2009; Calabrese et al., 2011). Such variation has been

observed in our experiments with the leech heartbeat CPG network from an *in vitro* study of the

isolated nerve cord (Norris et al., 2011). In the isolated nervous system, there is a large

variability from animal-to-animal in the temporal and synaptic output of the CPG corresponding

to similar variability in the fictive motor pattern (i.e. the motor pattern produced by the heart

motor neurons in the isolated nervous system) (Norris et al., 2011). In other words, despite the

large variability of internal parameters, the fictive motor patterns were all functional; they were

recognizable as fictive heartbeat. From these results it was hypothesized that each animal arrives

at different constellations of network parameters that shape its functional output pattern,

suggesting that individual variation in CPG output will be reflected in the actual movements they

control.

To address this issue, *in vivo* studies were performed to measure individual variation,

through the use of imaging and tension measurements (Wenning et al., 2014). Together, with an

in vitro study (Norris et al., 2011) this *in vivo* work shows that the peristaltic and synchronous

beat patterns were reliably conserved in the heart motor pattern, but the individual variation

decreased from *in vitro* to *in vivo* preparations, specifically in one of the two beat patterns

(synchronous mode). This implies a stabilizing effect within the minimally dissected animal which was previously unobservable in fully isolated preparations. In an effort to bridge these two observations, the current study employed a hybrid experiment: measuring tension of two heart segments with intact innervations to the isolated nerve cord. This preparation allows us to explore the fictive motor pattern's motor output in an *in vitro* environment to determine whether animal-to-animal variability in fictive heartbeat is reflected in the heart constriction patterns of individuals without the stabilizing effect of an intact preparation such as the one in the *in vivo* study.

For this portion of the study we will focus on ipsilateral midbody segments 8 and 12 in semi-intact and fully dissected preparations. Segments 8 and 12 were chosen for consistency with previous experiments and to assess the coordination and motor patterns of the hearts, which can be inferred from the intersegmental temporal delay (Norris, et al., 2011). A force transducer was attached bilaterally to heart segments 8 and 12, allowing us to monitor the phase relations of the two sides across duty cycles in an unloaded, *semi-intact* setting. The chain of ganglia is studied *in vitro* in a normal saline bathing solution while still attached to a right hemi-segment of the leech body at segments 8 and 12, connected solely by the ipsilateral roots. Tension measurements from the ipsilateral segments were taken simultaneously with extracellular recordings from the corresponding heart excitor motor neurons [HE (8) and (12)]. For a comparison of preparations and methods used in this and previous studies, please see Table 1.

Together with previous studies, these experiments will help us understand the functional significance of variability in nervous function for a well-studied behavior as well as the motor contributions which shape the behavior in various experimental conditions.

Materials and Methods

Animal and bathing solutions

Adult leeches (*Hirudo sp.*), weighing 2-5 g, were obtained from the commercial suppliers Leeches USA, Westbury, NY, or Niagara Leeches (www.leeches.biz/contact) and maintained at 16°C in artificial pond water. Leeches were kept in artificial pond water, anesthetized in ice prior to dissection or imaging for 10 minutes, and bathed in leech saline solution (in mM): 115 NaCl, 4 KCl, 1.8 $CaCl_2$, 10 Hepes buffer, and 10 glucose; pH adjusted to 7.4; at room temperature (21-22°C) after dissection. The solutions were applied through a perfusion system during electrophysiological experiments.

Intact preparation and imaging of hearts in situ

The constriction pattern in intact leeches (*Hirudo sp.)* was imaged by pinning the animals down, ventral-side up, onto a clear resin-lined tray. We flattened the animals with a glass plate, held in place by a glass cover and stabilized by screws. The tray with the intact, flattened leech was placed onto a platform with an opening on the bottom, allowing fiber optic lights to illuminate from below. The HD video camera was placed parallel above the tray. Once the areas around the leech are covered with dark paper, the camera can record the main bilateral circulatory vessels–the hearts –of the trans-illuminated leech with sufficient light and contrast. The leech was imaged for about 10 min so that 2-3 switch cycles of the peristaltic/synchronous mode will have occurred.

Video recordings of approximately 10 minutes were obtained for each animal, capturing segments 1 to 7 simultaneously. We used a Canon Vixia HF200 High Definition Camera (PF30 progressive, 30 f/s, MXP 24Mbps) (http://www.usa.canon.com) (Wenning et al. 2011; Wenning

et al. 2014). The bathing solution around the leeches was around 25 °C by the end of the procedure, which lasted 20-25 minutes.

Image processing is described in detail in Wenning et al. (2011) and Wenning et al. (2014). In brief, movies were converted into an AVI format readable by a custom MATLAB program (http://www.mathworks.com) using the Emicsoft MST Converter (http://www.emicsoft.com). The MATLAB suite detects the rhythmic light intensity changes of red blood filling the hearts. These optical signals were observed through user-defined regions of interest (ROIs; polygons) drawn around the heart segments, bilaterally, in each video clip. Absolute values of the digitized signals depended on the size of the analysis windows and on the signal-to-noise ratio of the optical signal obtained in a given heart segment. More importantly, the average intensity value of each ROI in each frame was plotted versus the frame number (i.e., the time) in the sequence, thus giving us phase relations across segments(Fig. 4).

Semi-intact preparation

Leeches anesthetized in ice for 10 minutes were stretched and pinned, dorsal-side up on a clear resin-lined dish. An incision was made along the animal's dorsal length, starting from around the midbody ganglion 14 and cutting towards the anterior side. Crop was removed and the hearts on both sides of segments 8 and 12 were exposed from surrounding tissues (Fig. 5). Segmental bladders were deflated without disturbing the nearby heart innervations. Each of the four bilateral heart segments was attached to force transducers. The entire experiment lasted 20-30 minutes and the tension recording sessions lasted approximately 10 minutes.

Tension measurement

Tension was measured using a semi-isometric, strain-gauge UFI Model 1030 Force Transducer (UFI Corp; http://www.ufiservingscience.com/model_1030.html).Force transducers were placed at a 45° angle on the micromanipulator stand, perpendicular to the preparation dish. A cotton thread (10 cm) was attached to the force transducer steel leaf at one end and an L-hook constructed from a Minutien pin (0.1 mm) at the other. Before adjustments to the thread length were made, the steel leaf was placed over the heart tube segment to be measured using the micromanipulator.

L-hooks produced more robust tension signals than rounded hooks due to their pronounced, sharp bends (Fig. 6). Hooks were directly inserted into the heart tube for this type of measurement, preferably near the segmental nephridium, avoiding the valve junction where afferent vessels adjoin the hearts, which produces competing peripheral signals (Jellies and Kueh, 2012). In the reduced preparation, this afferent interference was addressed by surgical removal. The hook's point made its first insertion contact from under the heart tube and pierced out through the top, taking care to incorporate the entirety of the bend into the tube. Thread length was adjusted to pull the transducer away longitudinally from the preparation while hooked onto the hearts.

Reduced preparation

Leeches anesthetized in ice for 10 minutes were stretched and pinned, dorsal-side up on a clear resin-lined dish. The dish has a built in ice chamber to keep the preparation in optimal condition throughout the dissection process. An incision was made to dorsally expose the animal and remove the crop covering. We exposed the ganglia chain from midbody segments 3 to 13

and cut all segmental nerves except the hearts on the right side of segments 8 and 12 were exposed with innervations to their respective segments kept intact. Hearts from adjacent segments (i.e. segments 7 and 9, 11 and 13) were also freed from surrounding tissue and were cut to half their segmental length, with their afferent vessels and valve junctions to the hearts completely removed (Jellies and Kueh, 2012). The body wall segments with the exposed hearts (and their attached half-adjacent segments) were subsequently cut out of the leech (see Appendix Figure 2).

The preparation (isolated chain of ganglia from segment 3 to 13 with heart segments 8 and 12 attached) was transferred to a preparation dish (10 cm) and laterally flipped to pin the ganglion ventral-side up, and the accompanying body segment (now on the left side of the chain) was vertically flipped and pinned skin-down so that the heart tube was visible. The anterior right packet of the ganglia of both segments was desheathed, leaving the neuronal cell bodies exposed to the external solution. The end product is an isolated chain attached to two right hemi-segments of the leech body with innervated hearts, connected solely by the ipsilateral roots (Fig. 7).The dish with the pinned preparation was transferred to the rig, illuminated from below using a dark-field condenser and continuously superperfused with saline solution (1.67-2.08 ml/min).

This biological preparation is an extension of the preparation used in the Appendix, which was modified from ones in previous studies by Nicholls & Baylor (1968) and Mason & Kristan (1982). The entire dissection process took from 2 ½ to 3 hours.

Electrophysiology and recording techniques

The electrophysiological techniques used for the reduced preparations are similar to the extracellular recordings outlined in Wenning et al. 2014. Electrodes were pulled on a

Flaming/Brown micropipette puller (P-97, Sutter Instruments; http://www.sutter.com) from borosilicate glass (1 mm OD, 0.75 mm ID; A-M Systems; http://www.a-msystems.com). For extracellular recordings, suction electrodes were filled with normal saline and placed in a suction electrode holder (E series, Warner Instruments; http://www.warneronline.com). To ensure a tight fit between cell and electrode, electrode tips were drawn to approximately the diameter of the motor neuron somata (30 μm). The electrode tip was brought in contact with the cell body and light suction was applied until the entire cell body was inside the electrode. Extracellular signals were monitored with a differential AC amplifier (model 1700, A-M Systems) at a gain of 1,000 with the low- and high-frequency cutoffs set at 100 and 1,000 Hz, respectively. Noise was reduced with a 60-Hz notch filter. A second amplifier (model 410, Brownlee Precision; http://www.brownleeprecision.com) amplified the signal appropriately for digitization. Recording were stable for up to 60 minutes.

Data acquisition and analysis

The data acquisition techniques are similar to those outlined in Wenning et al. 2011, as well as under the Appendix: Materials and Methods. Data were digitized (>5kHz sampling rate), using a digitizing board (Digi-Data 1200 Series Interface, http://www.moleculardevices.com) and acquired using pCLAMP software (http://www.moleculardevices.com) on a personal computer.

The constriction patterns of the individual heart segments were analyzed for period and phase using digitized optical signals and custom-made Matlab software (detailed in Wenning et al. 2004). Phase was defined as the delay between the maximum rate of rise (previously, "systole") (Fig.8) in one segment and that of the phase reference divided by the period. The

phase reference was the peristaltic Heart(7)in the intact anterior analyses (optical signals) and Heart(8) in the semi-intact and reduced preparations (tension recordings).

To measure extracellularly recorded spike trains to determine the heart motor neuron activity pattern and phase relations, we recorded simultaneously from the HE(8) and the HE(12) motor neurons. Spike detection and phase analysis were performed offline using custom-made MATLAB software (MathWorks).Phase was defined as the delay between the middle spike of a neuron's burst and the middle spike for the HE(8) motor neuron burst (phase reference) divided by the period.

In order to analyze burst characteristics–period, duty cycle, and intraburst spike frequency and phase –spikes were grouped into separate bursts. After an interspike interval ($\geq$1 s) elapses without any spikes detected, the next spike event was identified as the first spike of the next burst. Groups of less than five spikes were not considered as bursts.

With these measures, the motor neuron firing pattern and heart contractions components can be quantified, allowing for a correlational analysis between the two using programs such as Microsoft Excel. Importantly, these measures can be correlated with the measures of the actual heart constriction pattern.

Results

Phase relations of the hearts in the front segments

As shown in Figure 9, adult leeches (n=3) were pinned and trans-illuminated to provide sufficient color contrast for the video recording. We drew numerically color-coded polygons over the hearts near the bladders over each segment. Using different sizes of polygons provided the best results, with larger polygons yielding more robust signals for frontal segments 4-7 and smaller ROIs better-suited for the shorter intersegmental distance between the frontal segments 1-3. Within the 10 minute recording, the leech passes through 2-3 switch cycles, allowing us to compare phase bilaterally for both constriction modes.

Plotting and overlaying the heart segment phases show distributions across peristaltic and synchronous mode across segments (Figure 10). The anterior segments 3-7 conform to normal patterns of peristalsis (rear to front) and synchronous (nearly simultaneously), as confirmed by previous studies (Calabrese et al., 1995; Wenning et al., 2011). Taken separately, segments 1-3 appear to follow a slightly different pattern in both modes. There is also a greater degree of overlap in phase distributions between the peristaltic and synchronous modes, with a larger distribution variability noted for the synchronous mode.

Tension measurement of hearts in the semi-intact preparation

Originally, we attempted the semi-intact study with the use of the same optical signals used to analyze the intact video recordings. However, the dissection procedure caused too much blood loss within the animal's hearts, gradually reducing the optical signals over the course of the experiment. Force transducers were used instead to measure the tension caused by each heartbeat constriction (n=7), as done for the minimally dissected preparations in Norris et al., 2011. In

Figure 11, the bilateral phase relations of the heart segments referenced to the peristaltic segment 8 are plotted to show their distribution and variability within one animal across switch cycles. This figure also includes an actogram showing each heart beat cycle, plotted as the time of maximal rate of rise, on a raster scale, which is the averaged period. The double plotted actogram allows for a continuous representation of the recording, allowing the viewer to see individual phase relation by segment and side, phase shift across the switches, and precise time of switches across the system.

Figure 12 compares the variability of intersegmental phase differences of the semi-intact peristaltic mode with that of the fictive patterns (n=15) (Norris et al., 2011) and intact animals(n=13) (Wenning et al., 2014).In the peristaltic mode, the phase difference between heart segments 8 and 12 of hearts loaded with blood (minimally dissected and intact animals) differs significantly from that of empty hearts (semi-intact animals) ($p \leq 0.02$; two tailed unpaired t-Test) as well as the heart motor neurons (recorded in isolated nerve cords) ($p \leq 0.002$) (Wenning et al., 2014). Likewise, there is no difference in phase progression between heart motor neurons and empty (dissected) hearts. Significantly, no differences between these three different preparations were found in the synchronous mode (data not shown).

Physiological controls of the reduced preparation

We performed two control experiments to confirm the physiological connectivity between the chain of ganglia and the innervated body wall portions in the reduced preparation (Fig. 13). For one control, the connective between ganglia 5 and 6 was cut at the beginning of the recording. HE motor neurons became no longer coordinated with each other, and started tonic firing. Accordingly, the hearts lost bilateral coordination and, with no dependable motor input,

eventually started myogenic contractions. These observations were expected due to the loss of

connection within the core CPG interneurons (1-7) which are responsible for the timing and

coordination across the switch cycles as well as periodically inhibiting the heart motor neurons

(Calabrese et al., 1995). Also in Figure 13, the innervation between ganglion 12 and its

accompanying body wall with segmental heart was severed in a separate preparation. As

expected, the cell discontinues firing immediately after the cut, and the hearts eventually became

myogenic (period = ~50-60 sec).

Discussion

Characterization of constriction patterns in the front midbody segments

As mentioned before, plotting the phase relations between the front segments yielded some interesting patterns. While the frontal segments 3-7 are aligned to normal peristaltic and synchronous patterns, segments 1-3 appear to follow a slightly different pattern in both modes (Fig. 10). Thompson and Stent (1976a) established many years ago that the rhythmic driversof the hearts, the HE motor neurons, are located within midbody ganglia 3 to 18 but are absent from the two frontmost (and rearmost) ganglia. Without heart motor neurons of their own, segments 1 and 2 are innervated by segment 3's HE motor neurons.

The optical signal analysis provides new insight into the nature of this relationship between motor and constriction patterns of the front region. A larger degree of phase distribution overlap occurs between the plotted peristaltic and synchronous phase values, although the peristaltic maximal rate of rise still occurs substantially before that of the synchronous mode in phase. One possible explanation may be that the interconnected loop of the leech circulatory system creates a carry-over effect near the head as peristalsis contracts blood forward from the rear. Similar to the study on the rear segments (Wenning et al., 2011), the anterior constrictions differ in phase relations to those in segments 3-15 but seem to be coordinated with the core CPG output; however, the underlying synaptic mechanics responsible for this anterior difference cannot be definitely stated until further electrophysiological studies are conducted.

Limitations of the trans-illumination approach

The main limitation to this study concerned the rarity of leeches transparent enough (<5%) to perform the trans-illumination. Previous studies with juvenile leeches (Wenning et al., 2003)

did not have this problem due to inherent transparency in the juvenile population. Adult leeches lose their transparency over development, often forming thick, dark lines on the superficial layer of the body wall area covering the hearts. Although an electrophysiological component was originally intended for these experiments as well, the lack of subjects and the intensity of the ensuing procedures did not create optimal conditions.

Comparison of semi-intact segmental phase relations

By measuring constrictions of the unloaded (blood-less) hearts in the semi-intact dissection (Fig. 11) and comparing the phase values to those of previous studies (Fig. 12), we have demonstrated that these hearts have similar phase relations to those of the fictive motor pattern. Our focus then shifted to the peristaltic phase distribution differences between the semi-intact and intact preparations. Wenning et al. (2014) propose that the pressure within the heart tubes causes a loading effect over the intact system, delaying constrictions and amplifying peristaltic phase differences. In the current study, we attempted to observe the peristaltic delay through a condition reversal: experimentation in the open, semi-intact dissection removed this loading effect from the ensuing blood loss. Statistical analyses confirm that empty hearts constricted more closely in line with the CPG-governed motor patterns, such as those in the isolated preparation. Synchronous values remain similar throughout preparations.

A continued study should incorporate electrophysiological recordings to track the burst activity of HE motor neurons as the hearts themselves constrict. Recordings were not possible in this particular dorsal preparation because of the ventral access needed for HE motor neurons.

Comparison of phase distributions in the reduced preparation

Analysis of the heart phase relations in the reduced preparation implies a similarity of the reduced preparation peristaltic phase range to those of the isolated and semi-intact preparations. This adds further support for the loading effect of hearts in the peristaltic mode of intact preparations. It is proposed that within a closed system, blood can only be transferred to a finite number of spaces, intermittently causing delay in constriction as blood propels from the rear to front in peristaltic mode.

Several experimental and offline accommodations were necessary to accurately acquire and analyze data from the reduced preparation recordings. Some early experiments contained recordings of the actual HE signal along with activity from peripheral spiking (not shown).Recently, Jellies and Kueh (2012) discovered that this peripheral activity originates from the afferent vessels and valve junctions to the hearts. Cutting away these physical sources from the heart tubes subsequently eliminated the peripheral spiking from the HE recordings (Fig. 14). Most heart recordings also exhibited high levels of oscillation in the baseline throughout the recording, creating an added confound to the analysis. The baseline shifts are thought to be from movement of the body wall caused by muscle contractions. This issue was mainly addressed by implementing a custom MATLAB filter program which retained the phase value and maximum rate of rise for each constriction while re-plotting the absolute values without the shifts.

<u>Conclusion</u>

      Findings from the front analyses of segments 1 and 2 indicate a different constriction pattern from other midbody segments. Although the control of HE(3) motor neuron innervation of constriction in heart segments 1 and 2 remains unknown, a different phase relationship across the switch cycles remain evident. If similar to the findings in the rear coordination, it can be stated with reasonable certainty that heart segments 1-3 remain entrained to the motor pattern of the core CPG (Wenning et al., 2011). Further electrophysiological and modeling studies will be needed to establish the network dynamics that influence this pattern.

      Comparing the intersegmental phase relations of segments 8 and 12 show a highly conserved pattern of distinct constriction patterns associated with the two coordination modes, across the different preparations. Particularly in unloaded experimental conditions, the peristaltic heart distribution remains similar in the semi-intact and chain-preparations of this study, as well as the isolated chain and minimally-dissected preparations used in previous studies inthe Calabrese Lab. Synchronous phase values are similar in variability across all preparations compared here and previously (Norris et al., 2011; Wenning et al., 2014).
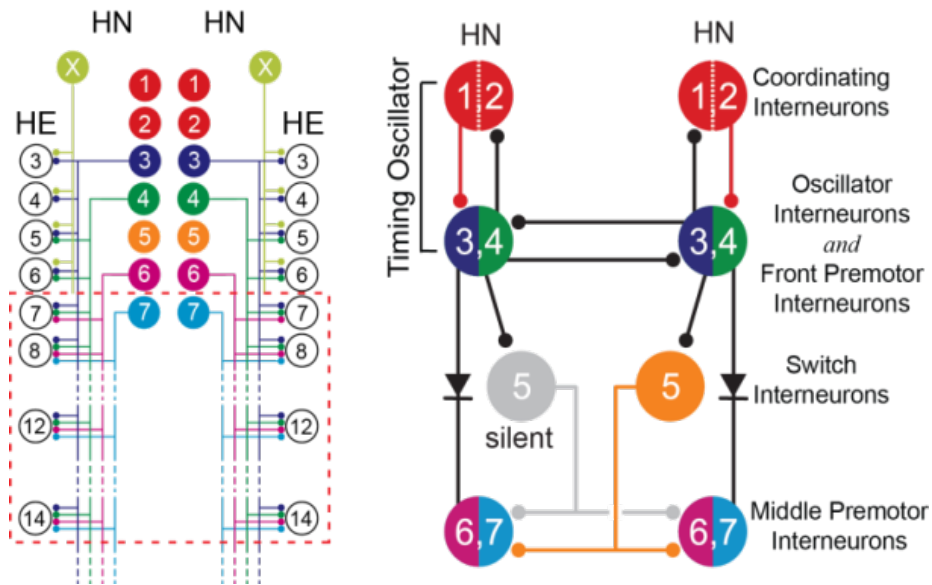
      The efforts of this study help to impart a greater understanding of the underlying network parameters that guide the rhythmic heartbeat. The dissected preparations explored previous observations on the physical conditions of a biological preparation and the change in phasing an open or closed circulatory system caused. New information on the front heart segments also suggests an added dimension of complexity to the well-established paradigm in the midbody segmental hearts. Together, these experiments provide additional insight into the heartbeat system, allowing for more accurate future modeling studies.

List of Figures

Table

Figure 1

Left: Bilateral circuit diagram of all premotor heart (HN) interneurons of the core CPG

(identified HN(3), HN(4), HN(6), HN(7) and unidentified HN(X)) and their pattern of synaptic

connections to ipsilateral motor neurons (HE) in HE(3) - HE(14). Right: The circuit diagram

illustrates the synaptic connections among the heart interneurons that compose the core network

of the heartbeat CPG. One HN(5) interneuron is grayed out to signify that only one of them is

active in bursts at a time, corresponding to the two coordination modes of the CPG. Cells with

similar input and output connections and function share a circle. Lines indicate cell processes,

small colored/black circles indicate inhibitory synaptic connections and diodes indicate electrical

connections. Interneurons and motor neurons are indexed by side and midbody segmental

ganglion number e.g. HE(L,3) - HE(R,18). (from Norris et al., 2011).

Image redacted due to copyright laws
Image can be accessed at this link:
http://nelson.beckman.illinois.edu/courses/neuroethol/
models/leech_swimming/leach_anatomy.gif

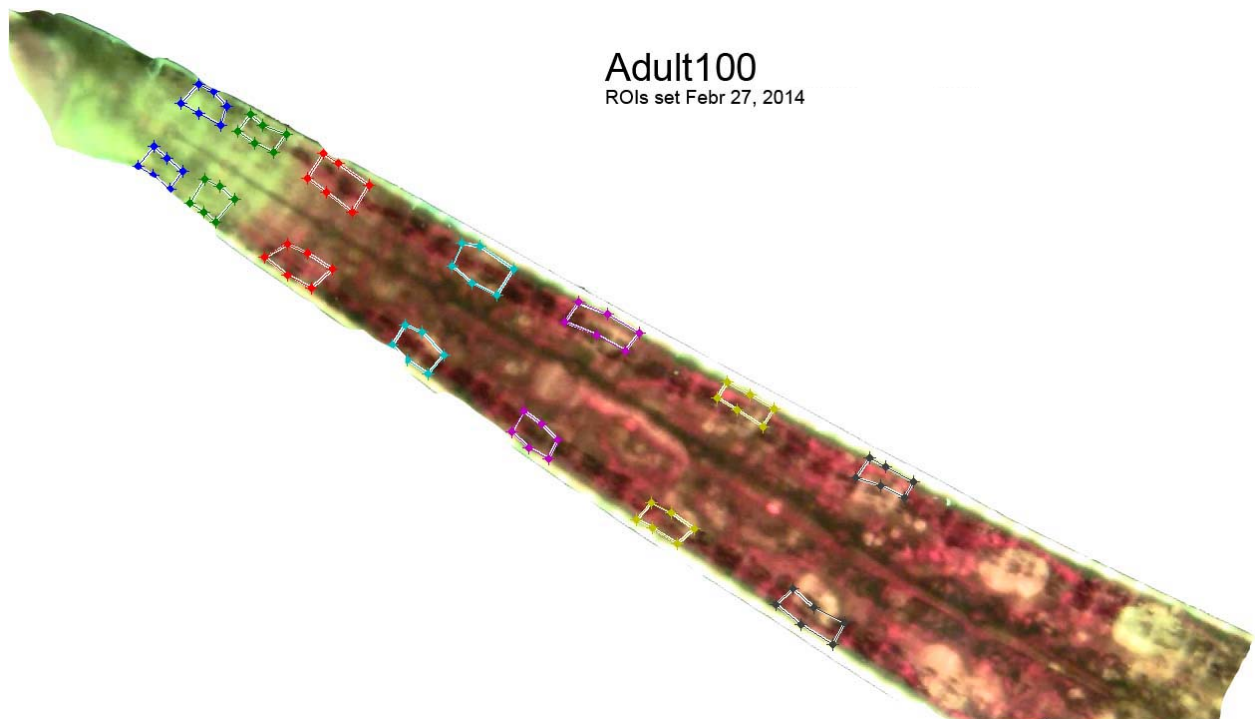**Figure 2**

Midbody segmental ganglia and cross section of a medicinal leech. The leech contains 21

midbody segmental ganglia connected by a continuous nerve cord, terminated by head and tail

ganglia on the ends. The cross section shows the four different layers of musculature in the leech

body wall. The chain of ganglia is contained within the ventral sinus. (from Blackshaw &

Nicholls, 1995).
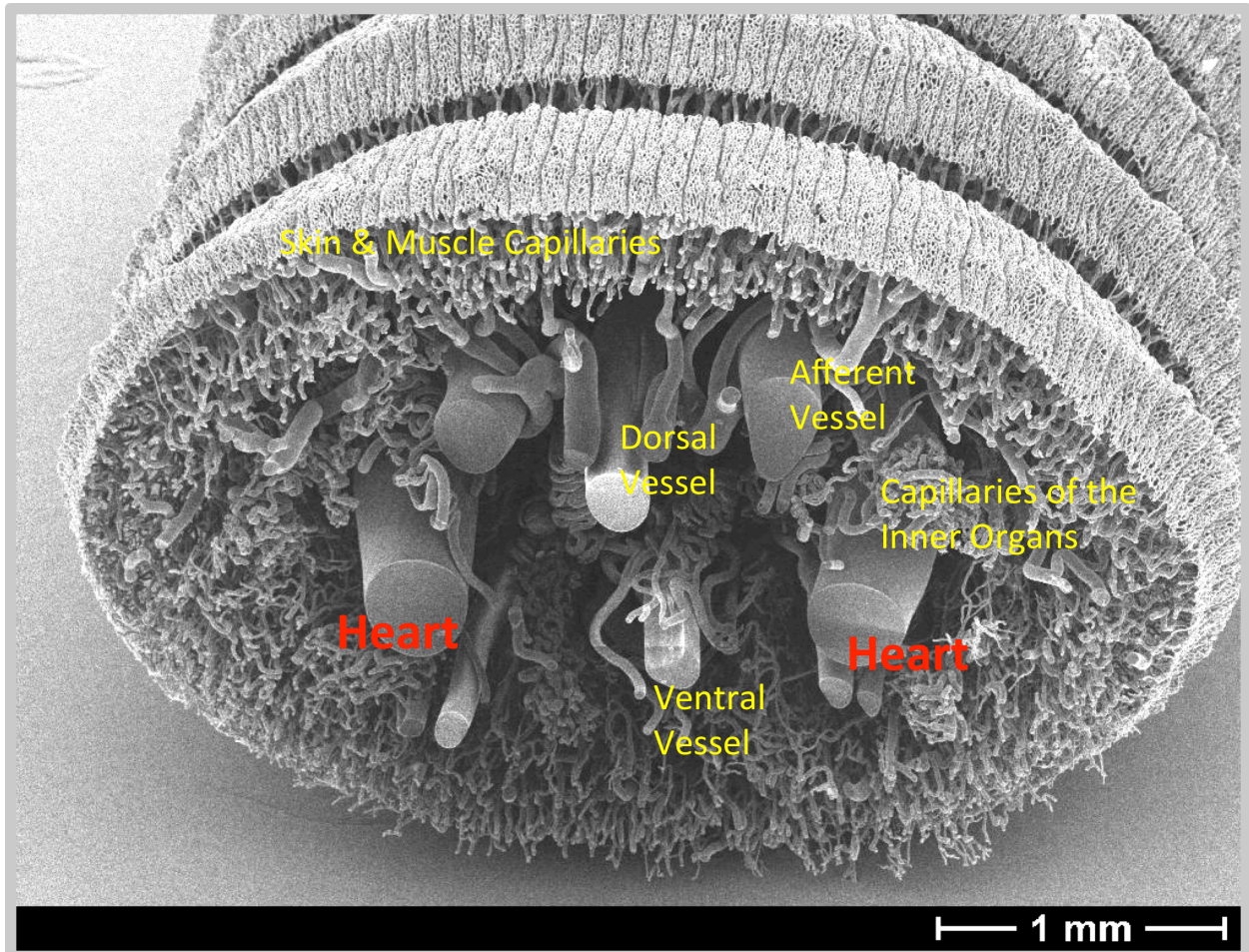
Figure 3

Cross section corrosion cast of leech vasculature and four main vessels. The focus of the current study is on the lateral vessels, also referred to as the heart tubes. The two, tubular hearts are located along the body axis and consisted of segmental iterated sections. They are coordinated by segment and differently on the two body sides, alternating between the peristaltic and synchronous patterns signaled by the CPG. (from Wenning and Meyer, 2007).

Figure 4

In situ recording of trans-illuminated leeches with user-defined region of interest (ROI) polygons. Segments 1-7 are labeled for Adult100, the first individual used in these experiments. Windows are drawn over the clear bladders to create robust optical signals from the color contrast of red blood passage during filling and constriction.
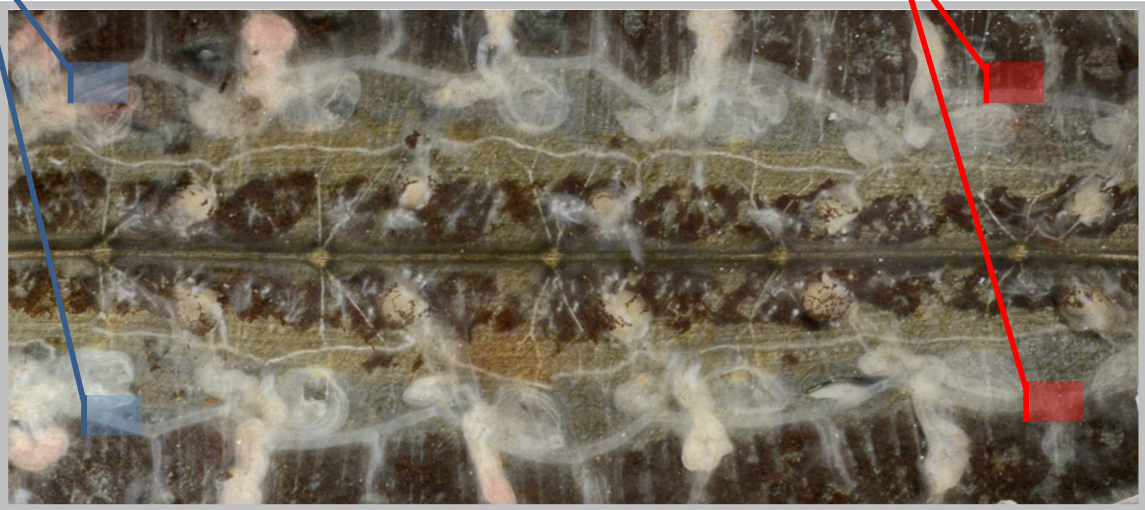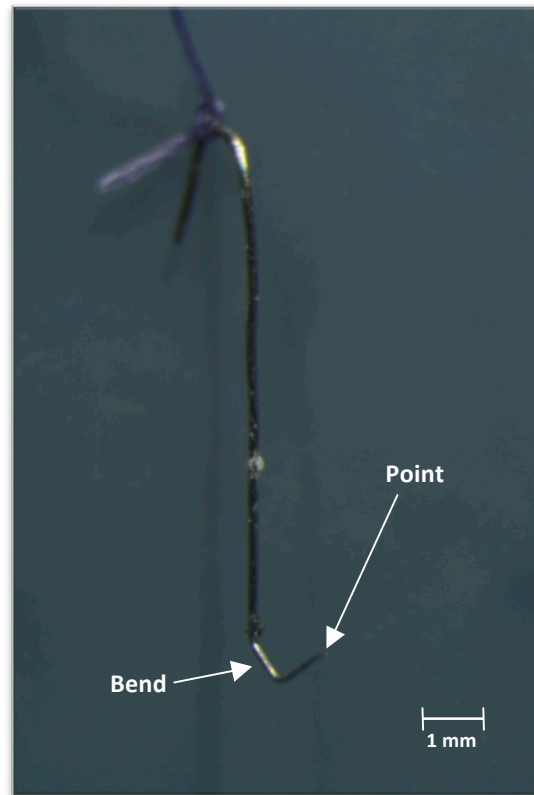
Figure 5

Dorsally pinned, semi-intact preparation of leech segments 8 to 12. The crop covering and tissue surrounding the heart tubes were removed. Hearts are hooked to the force transducers in the shaded areas of segment 8 and segment 12.

Figure 6

Minutien pin L-hook hand-constructed using forceps. The hook is tied to a force transducer metal leaf with a thread.
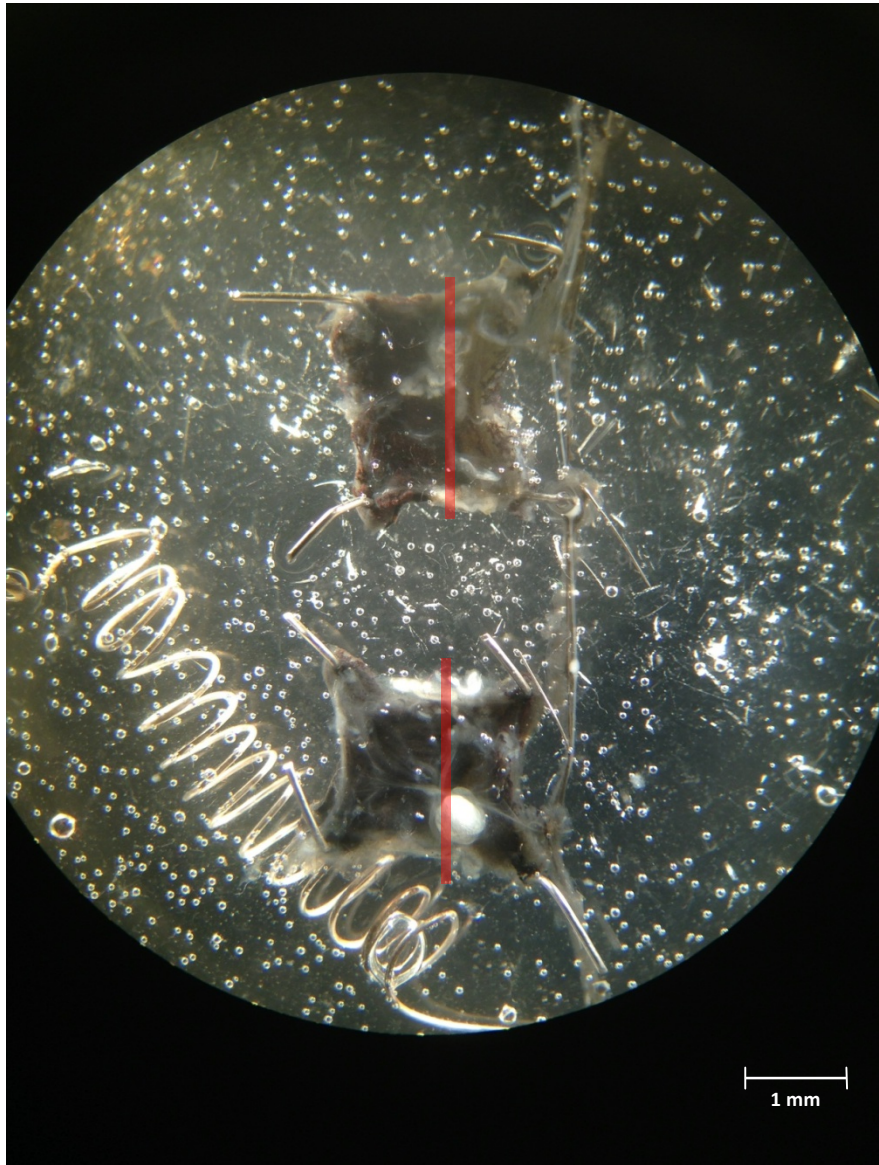
Figure 7

The reduced preparation, consisting of an isolated chain of midbody segmental ganglia with ganglia 8 and 12 innervated to two portions of the dorsal-right body wall and respective segmental hearts. The heart segments 8 and 12 are shaded in red. The preparation is designed to simultaneously allow electrode recordings from HE motor neurons located in each segmental ganglion and tension measurement from the heart segments on the same side. Image was taken using an iPhone 5 camera through a microscope viewing lens.
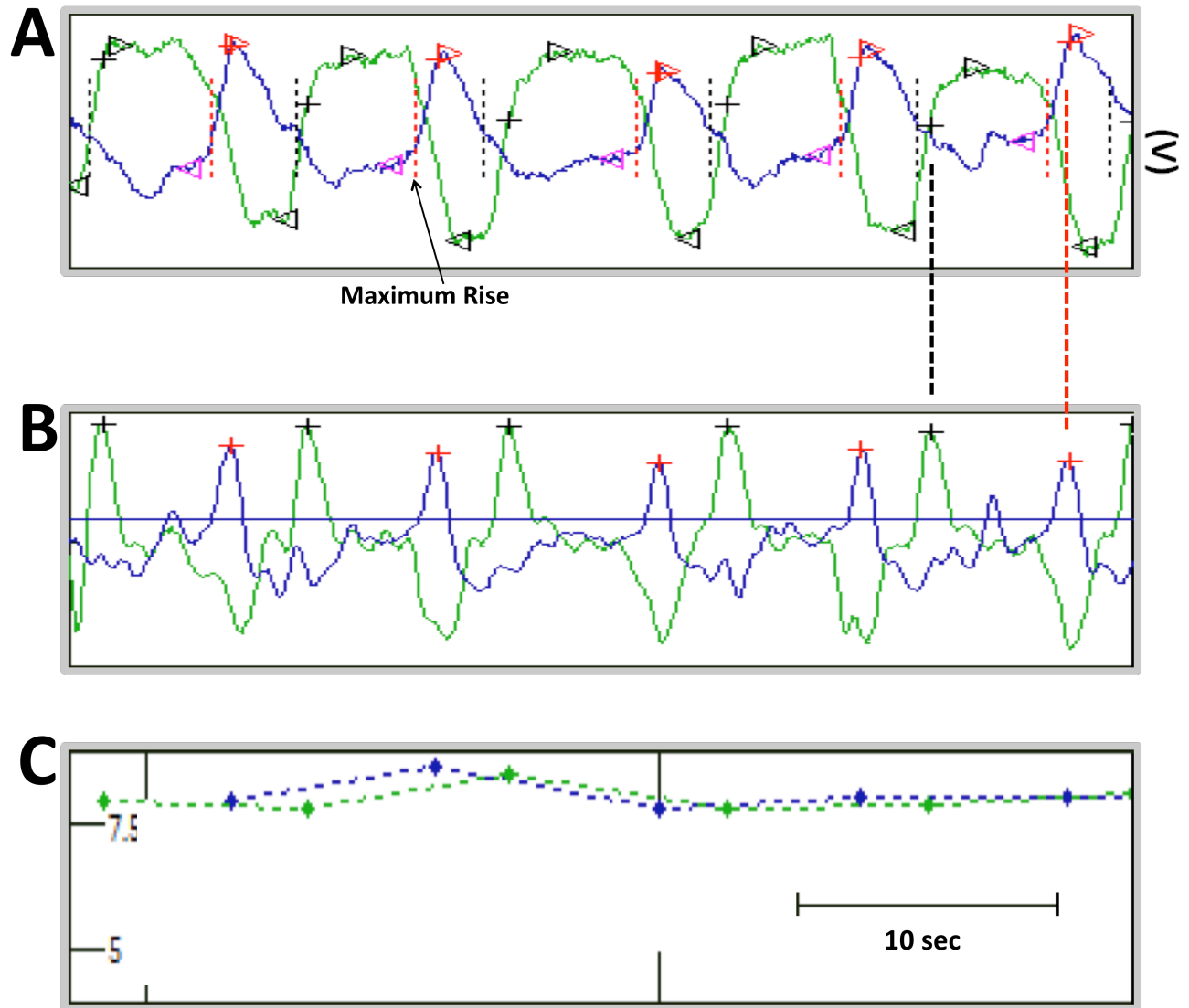
Figure 8

Optical signal and tension analysis of the phase reference and a heart segment. Both types of

signals were analyzed using the same custom MATLAB program. **A)** Absolute values (in V) of

the signals from the two segments for phase comparison. **B)** The first derivative of the signals in

A: the peak of the upward slope corresponds to the maximum rate of rise of the constriction

[formerly called systole (Wenning and Meyer 2007) phase marker).**C)** Cycle period across beats.
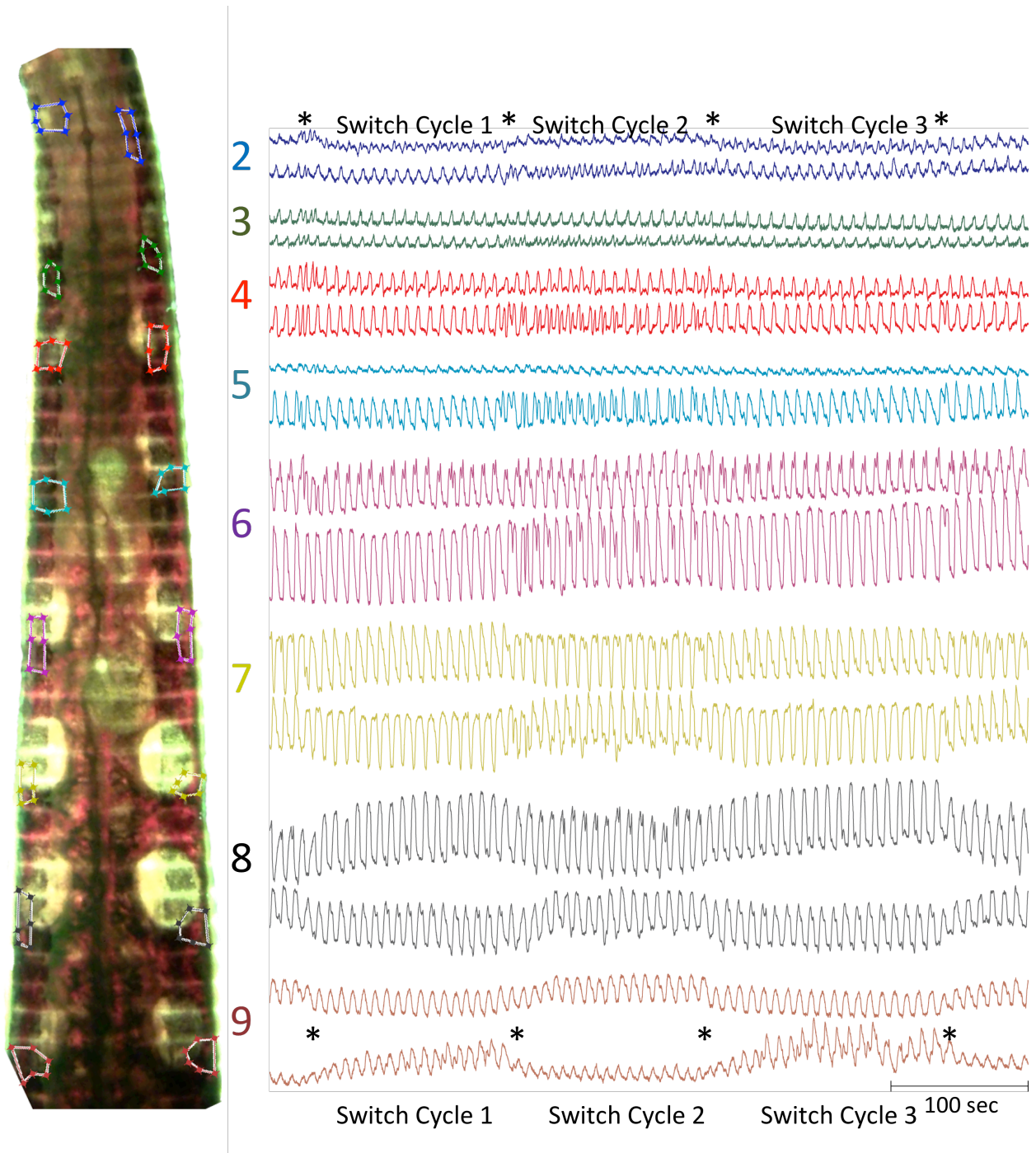
Figure 9

Eight pairs of analysis windows drawn around corresponding areas of 8 pairs of heart segments in a trans-illuminated adult leech (left) yield the corresponding optical signals (right). Asterisks indicate the 4 switch cycles (#'s 1-3) in coordination mode in this experiment.
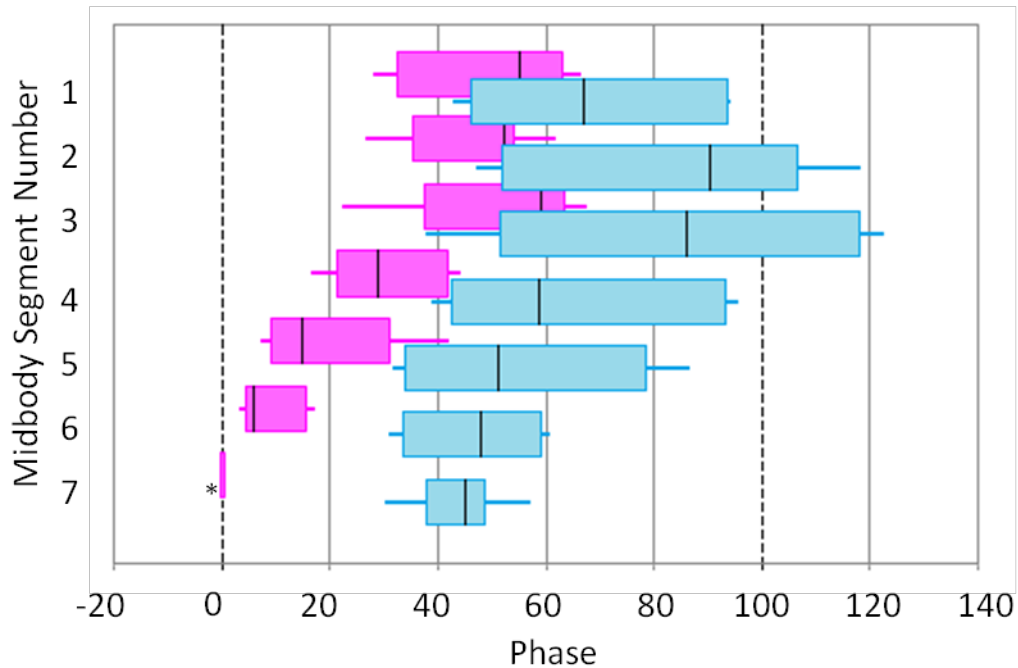
Figure 10

Phase relations of heart segments (maximal rate of rise) across switch cycles in the front of the leech (midbody segments 1-7). The peristaltic and synchronous phase distribution with interquartile range and median values of both sides is overlaid here. *The peristaltic 7 is used as the phase reference. Peristaltic, as well as synchronous, phase distributions in segments 3-7 show the rear-to-front progression seen in the same modes of other preparations.
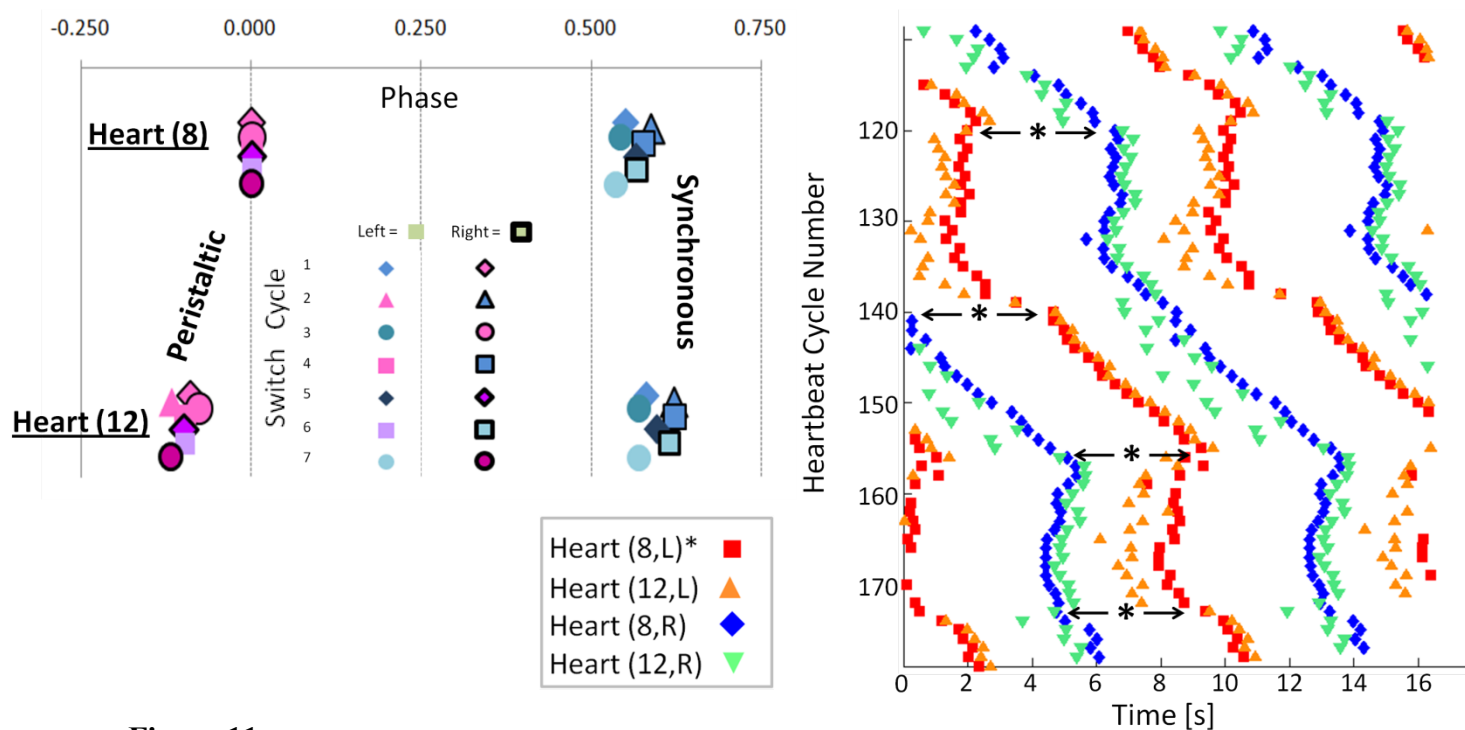
Figure 11

Phase relations in heart segments 8 and 12 across switch cycles. (Left) Intersegmental phase relations are similar on both sides with little variability over the seven switch cycles. Each point is the average of all beats within a switch cycle. (This animal had about 18-20 heartbeats per switch cycle).Heart segment 8 on the peristaltic side is the reference and assigned 0 phase. Overlapping points are slightly displaced vertically for visibility. (Right) With the same individual, tension signals from the heart segments (L, 8; L, 12; R, 8; R, 12) shown as an actogram. Each symbol represents the maximal rate of rise of one heart. Heartbeat cycles were plotted as the time of maximal rate of rise on a raster scale, which is the average period, and then double plotted (shifted up one raster point) for a continuous representation of the experiment (~10 min). The asterisks and arrows indicate switches of coordination modes. Right/left shifts in the signals indicate a decrease/increase of the cycle period. Note that all 4 segments were measured simultaneously in one preparation.
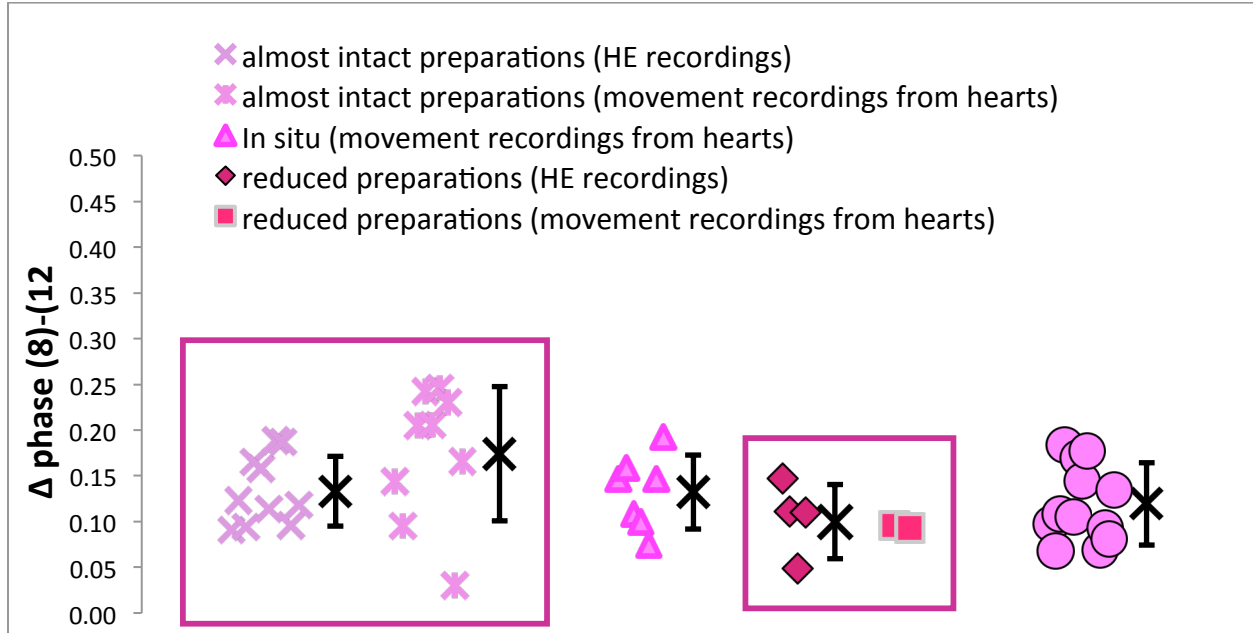
Figure 12

Comparing variability of phase differences in almost intact (minimally dissected) HE motor neurons and heart, semi-intact heart, reduced HE motor neurons and heart, and fictive preparations. In the peristaltic mode, the phase difference between heart segments 8 and 12 of loaded hearts (almost intact animals) differs significantly from that of empty hearts in dissected animals ($p \leq 0.02$; two tailed unpaired t-Test), in reduced preparations ($p \leq 0.008$) as well as the heart motor neurons (recorded in isolated nerve cords) ($p \leq 0.002$). There is no difference in the phase difference between heart motor neurons (fictive pattern) and empty hearts. No difference between these three different preparations was found in the synchronous mode (data not shown).Different plot groups enclosed by the same rectangle indicate that the phase relations were simultaneously obtained from the same individuals (data from Norris et al., 2011; Wenning et al., 2014).
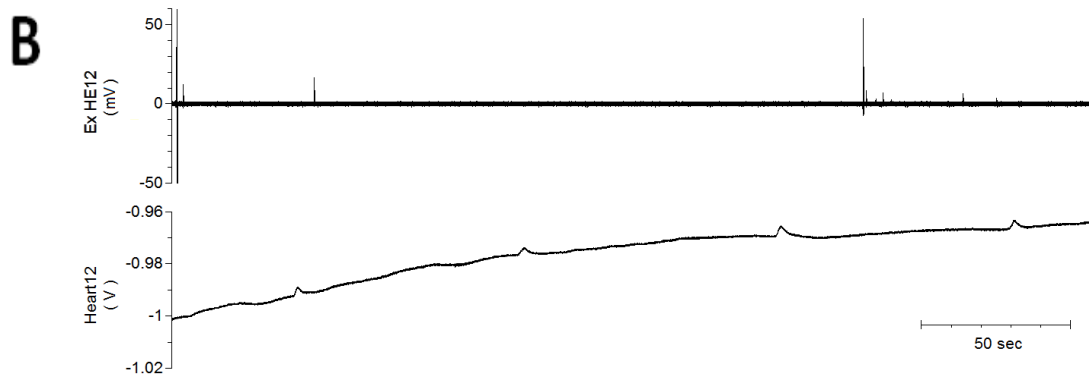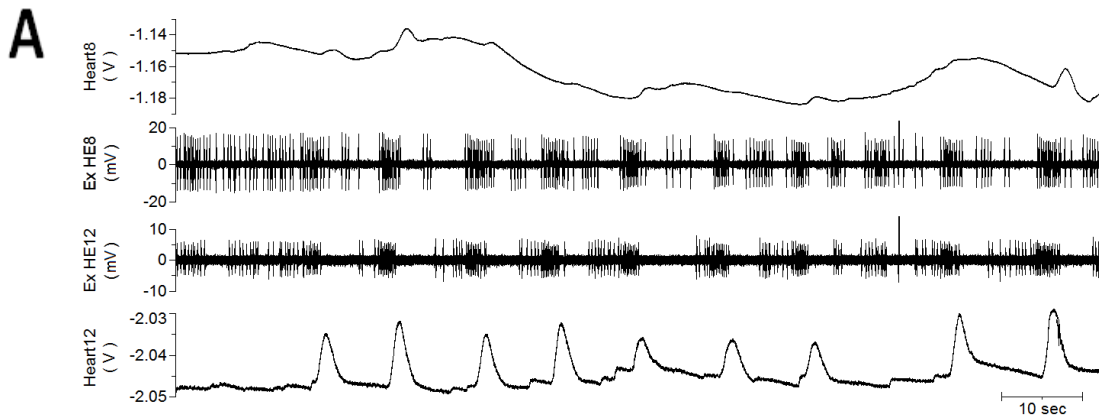
Figure 13

Physiological controls of the reduced preparation in segments 8 and 12. A) The connective between ganglia 5 and 6 was cut at the beginning of the recording. HE cells, and subsequently the hearts, are no longer coordinated with each other, and the motor neurons have stretches of tonic firing. The hearts eventually become myogenic. The four channels shown here are (in descending order) signals for heart(8) tension, HE(8) extracellular, HE(12) extracellular, and heart(12) tension. B) The anterior root innervation between ganglion 12 and its accompanying body wall with segmental heart was severed at the beginning of this recording. The cell discontinues firing, and the hearts become myogenic.
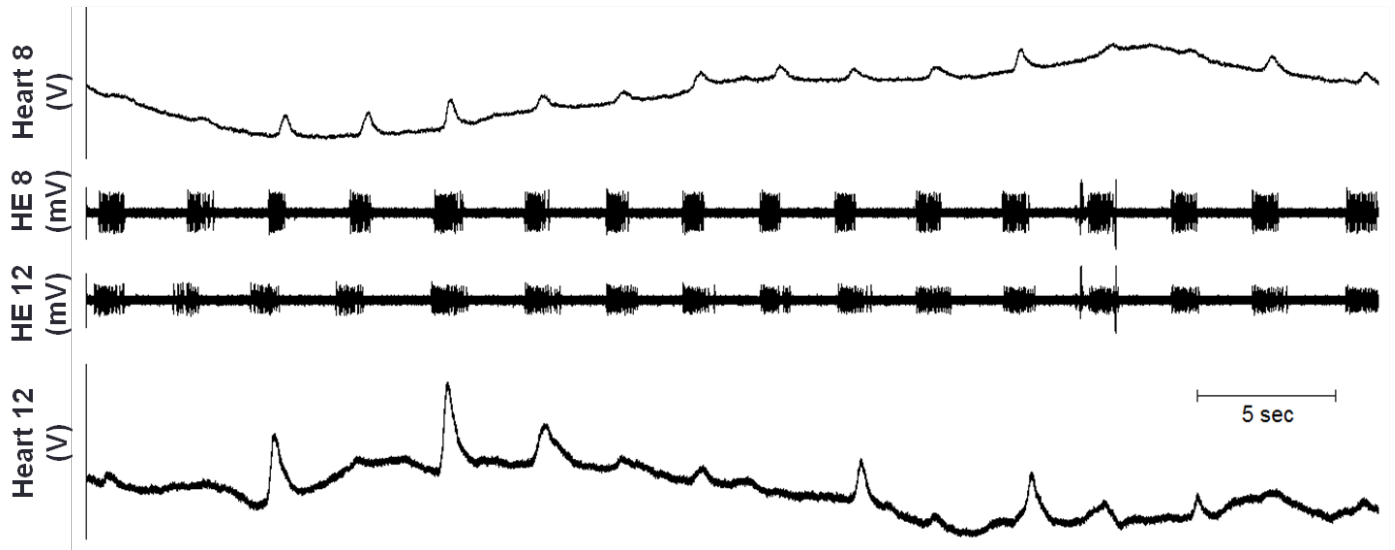
Figure 14

Extracellular recordings from HE(8) and HE(12) motor neurons along with tension movement recordings from heart segments 8 and 12.Removing the afferent vessels and valve junctions from eliminated the peripheral spiking from the HE recordings, as discovered by Jellies and Kueh (2012). Without the physical source for the peripheral activity, the reduced heart constrictions remained coordinated to their respective HE bursts.

Preparation Type	Method of Signal Acquisition	Physical Characteristics
Intact	**optical signals**	**No dissection; loaded hearts; used for front segments in this study**
Almost (minimally) Intact (*in vivo*)	extracellular recordings, optical signals, tension displacement	Minimal dissection (superficial cuts); loaded hearts
Semi-Intact	**optical signals, tension displacement**	**Dorsal dissection, crop removed; unloaded hearts**
Reduced	**extracellular recordings, tension displacement**	**Isolated chain and (2) attached body wall and heart segments**
Isolated Chain (*in vitro)*	extra- & intra-cellular recordings	Chain of ganglia; no hearts

Table 1

Experiments are sorted by preparation type, methods used in signal acquisition, and physical characteristics of interest. The preparations used in this study are bolded.

Appendix:

Effects of Stretch Stimuli on the Nonspiking (NS) and Touch (T) Cells in the Leech

By

Jason Kim

Emory University

International Research Experience for Science Students (IRES)

Martin Carbó-Tano, PhD.

Lidia Szczupak, PhD., Advisor

University of Buenos Aires, Ciudad Universitaria

Instituto de Fisiología, Biología Molecular y Neurociencias - CONICET

An appendix of
a thesis submitted to the Faculty of Emory College of Arts and Sciences
of Emory University in partial fulfillment
of the requirements of the degree of
Bachelor of Science with Honors

Program in Neuroscience and Behavioral Biology

2014

Notes on the Appendix

The experiments contained in this appendix were conducted at the University of Buenos Aires, Ciudad Universitaria in Buenos Aires, Argentina under the supervision of Lidia Szczupak, PhD., as part of a 10-week summer fellowship (June-August 2013) funded through Emory University's International Research for Science Students (IRES) Program. Contents of the appendix are unpublished original work, included here mainly to supplement and reflect the development of the methods and biological preparation used in the thesis work. This work uses the same model organism (*Hirudo sp.*) as used in the thesis.

Abstract- *A*

Using the medicinal leech (*Hirudo sp.*) as a model system, we investigated how different sensory parameters affect motor output. We explored the stretch sensitivity of neurons with projections from the nerve cord to the periphery. Using an isolated ganglion preparation with the nerve roots connected to one hemi-segment of the body wall, we investigated the effects of tension stimuli on the body wall while simultaneously recording intracellularly from a neuron in the corresponding segmental ganglion. We focused in particular on the responses of the nonspiking (NS) and touch (T) neurons. The NS neuron, which extends projections to the periphery, has actions on the entire population of motor neurons in the segmental ganglia and influences motor behaviors (Wadepuhl, 1989; Rela & Szczupak, 2007; Rodriguez et al., 2012). We explored the possibility that the NS cell acts as a stretch-sensitive mechanoreceptor. T cells are low threshold mechanoreceptors and their stretch sensitivity has been documented in previous studies (Nicholls & Baylor, 1968; Blackshaw, 1981), but specific characteristics have not been explored in greater detail. Stretch stimuli do not elicit a response from other neurons not thought to be stretch receptors, and these recordings served as electrophysiological and mechanical controls. Results from our different experimental conditions indicate that the NS neurons are not stretch-sensitive receptors but strongly indicate that they receive synaptic input from stretch receptors. On the other hand, the low threshold mechanosensory T cells were shown as robust velocity-dependent stretch receptors.

Appendix: Table of Contents

Introduction-*App*

Studies of mechanosensory neurons in the leech have had a long tradition. Owing to the simplicity of the nervous system in this organism, researchers have been able to maneuver and explore the various neurons in ways unfeasible in vertebrate models (Kristan et al., 2005).

In the pioneering study, Wadepuhl (1989) identified the extensive connectivity exhibited by the cell 151 in the segmental ganglia of the leech, a possible prerequisite in functioning as a regulator for electrically-driven activity (illustrated in Appendix Figure 1). These pairs of cells notably are electrically coupled to each other and have extension of neurites through the ganglion roots. They were further characterized by electrical coupling to virtually all excitatory motor neurons, "spontaneous" IPSPs, shifts in membrane potential, and the lack of Na^+-dependent action potentials (Wadepuhl, 1989; Rela and Szczupak, 2007). This last trait gave rise to its current name, the non-spiking (NS) cell. Spike-like activity is only elicited under specific conditions of the membrane potential (Rela et al., 2009). Rela and Szczupak (2003) demonstrated that excitation of motor neurons produced an inhibitory feedback loop from the NS cells, transmitted through rectifying electrical synapses back to the motor neurons. The widespread polarizing effects incurred on identified motor neurons solidified NS neurons as prime candidates for modulators of motor activity.

While the NS cells actively contribute to regulation of motor activity, they also receive synaptic input from mechanosensory cells (Wadepuhl, 1989; Rela and Szczupak, 2003). Specifically, the T (touch), P (pressure), and N (noxious) mechanosensory cells, have been studied in great detail in terms of organization and functional importance, are also known to run their axons to the through the ipsilateral nerve roots (Nicholls & Baylor, 1968; Blackshaw, 1981; Blackshaw, et al., 1982). Laverack (1969) also deduced the sensory endings of the first-order

mechanoreceptors to be in the superficial layers of the body wall by stimulating the animal and recording the evoked responses from mechanoreceptors. In addition, peripheral neurons located on the nerve roots were shown to be stretch receptors and the T cell is unique in that it has been the only one of the three primary central mechanoreceptors capable of detecting stretch (Blackshaw & Thompson, 1988). While the peripheral stretch receptors respond to tension with sustained hyperpolarization, the T cells were excited by this stimulus.

With these similar projections to the peripheral sensory field, we explored the possibilities of NS acting additionally as a stretch-sensitive mechanoreceptor. Although the property of stretch sensitivity has been well documented in these previous studies, specific characteristics of the T cell's stretch sensitivity have not been explored in greater detail. By using an isolated ganglion preparation with the root connection to one hemi-segment of the body wall intact, we investigated the effects of tension stimuli on the body wall while simultaneously recording from either an NS or T cell. The application of tension mimicked a longitudinal stretching effect on the epidermis and surrounding tissue whereas previous studies, specifically in T cells, stretched the longitudinal muscle itself (Blackshaw & Thompson, 1988). Results from our different experimental conditions indicate that the NS neurons are not stretch-sensitive receptors but strongly indicate that they are synaptically connected to stretch receptors. Experiments with the T neuron indicate a specific sensitivity to tension application velocity. These results also add to our observations on the T cell's low-threshold effect of activation to stretch stimuli.

Materials and Methods- *App*

Biological preparation

        Adult medicinal leeches (*Hirudo sp.*), weighing 2-5 g, were obtained from the commercial supplier, Leeches USA, Westbury, NY, and maintained at 15°C in artificial pond water. Leeches were anesthetized in ice prior to dissection and then pinned to a silicone elastomer (Sylgard) dish, dorsal-side up.

        We focused exclusively on the midbody segments 8 and 10. Isolated ganglia were attached to a right hemi-segment of the leech body, connected solely by the ipsilateral roots (see Appendix Figure 2). Tissue connectives surrounding the nerve roots were dissected away to allow a greater degree of autonomous mobility in the leech body segment during tension application while minimally disturbing the electrode position. Incisions into the body and nerve cord were made to maximize the surface area of one segment. The preparation was transported to a dish and flipped to pin the ganglion ventral-side up, and the accompanying body segment was pinned with its skin-side up. The skin was attached to the Sylgard by pins located along the posterior and lateral edges. A small anterior portion of the body segment was left un-pinned to allow for the force transducer's hook-placement. The sheath covering the ganglion was dissected away, leaving the neuronal cell bodies exposed to the external solution. The biological preparation was modified from ones in previous studies by Nicholls & Baylor (1968) and Mason &Kristan (1982).

Bathing solutions

        The ganglia and dissection preparation were bathed in a normal saline solution (in mM): 115 NaCl, 4 KCl, 1.8 $CaCl_2$, 1 $MgSO_4$, 10 Hepes, 10 glucose; pH 7.4; at room temperature (20-

23°C). To block synaptic transmission, we used a 10 mM Mg^{2+} solution made from 18 mL of $MgSO_4$ and 182 mL of normal saline. High Mg^{2+} was applied for 10 minutes and washed for 10 minutes with normal saline. The solutions were applied and washed through a perfusion system.

Electrophysiology

Intracellular somatic recordings were made with microelectrodes pulled from borosilicate capillary tubing (FHC, Brunswick, ME), filled with 3 M potassium acetate (resistance 20–40 MΩ). The electrodes were connected to an Axoclamp 2B amplifier (Axon Instruments; Union City, CA) operating in bridge mode. The intracellular recordings were digitized using an analog digital converter (Digidata 1320, Axon Instruments) and acquired using a commercial program (Clampex 9.2, Axon Instruments) at sampling rates of 5-10 kHz. All neurons recorded intracellularly were recognized by their soma location, electrophysiological properties. Most of our experimentation was done on the T_2 neuron, ipsilateral to the body wall segment.

Tension measurement

Tension was applied using a Grass Model FT03 Force Displacement Transducer (Grass Technologies). A 6-0 polypropylene monofilamentsurgical suture (PROLENE™; Ethicon, Inc.) was attached to the force transducer at one end and a J-hook constructed from a Minutien pin at the other. No springs were used as an intermediate to remain sensitive to the range of force applied on the tissue (0-10.6 g; 0-0.21 V). Calibration of the machine was done by incrementally adding weights of similar mass and comparing the electrical output of the transducer to the applied force for linearity (see Appendix Figure 3).

Data analysis

Recordings were analyzed using the Clampfit 10.0 software (Axon Instruments). A time integral of the response (response area) in the NS was measured for a 10 second window after the approximate start of tension. Due to the varying membrane potential of NS (Vm_{NS}), we set an averaged baseline at a period prior to the tension response. Other important values considered in analysis were basal tension, maximum tension attained (Δtension of absolute maximal and basal), slope of tension application, and Vm_{NS} before tension change.

Limitations and compensations in methodology

Several limitations were noted during the course of this study and compensated for to the best of our ability. The two major sources of limitations were mechanical and quantitative in nature.

The greatest hindrance to this study was the lack of precise tension application. All stimulations were done manually, thus interfering with rate of application and total force applied (illustrated in Figure 2). We used maximal tension attained (Δtension) as our primary measure of force application to compensate. All other mechanical modifications, such as range of force applied, were kept as consistent as possible during analysis.

The properties of the skin added another challenge to our study. After 10-15 recordings, possible damage to the epidermis could have occurred after repeated stretching. Adjustments were made to pin the tissue in a way that would not affect the electrode position while the body wall was being stretched. Much of the connective tissue surrounding the ganglion roots was removed, and the pins holding the stocking adjacent to the body segment were loosened to combat this effect.

As noted by Rodriguez et al. (2009), the variable nature of the NS membrane potential (Vm_{NS}) ultimately affected our quantitative evaluation of the response. Measurement of response area was chosen over that of response amplitude due to the response of the cell to sustained tension. This measurement would also equalize artifact effects across the experimental conditions.

Results- *App*

Experimental controls

The preparation consisted of a piece of body wall corresponding to approximately one hemi-segment, to which the ganglion was kept attached through the roots. To evaluate that the connection between the ganglion and the body wall was in good physiological state we stimulated the P and annulus erector (AE) neurons (Appendix Figure 4). Direct excitation of the annulus erector motor neuron produced contraction of the annuli muscles increasing the overall tension of the body wall. The P cell synaptically excites the longitudinal motor neurons and thus it also increased body wall tension. This control was performed before recording from NS and T cells.

As an additional control, we recorded from a T cell after crushing its axons (Appendix Figure 5). The T cells stopped responding to tension stimuli, indicating that the T cell response was not due to mechanical artifacts. Our initial observations and recordings were done in a normal saline solution.

NS response to body wall tension

A total of 12 different preparations (N=12) were recorded where tension was applied onto two distinct areas of the leech body segment: dorsal and ventral. This was accomplished by attaching the hook onto the dorsal and ventral portions of the leech skin. In relation to the isolated ganglion preparation, the ventral hook assignment was immediately adjacent to the ganglion. As a general note, whenever tension was applied, there were several resistance factors. Once maximal tension was applied, the skin naturally adjusted to the pull and lessened the amount of total force applied. Manually returning to basal tension also proved difficult due to

unknown natural mechanisms employed by the nervous system to contract the skin in response to stimuli.

As shown in Appendix Figure 6, we studied the effects of increasing tension applied to the body segment, at different rates of force increase. In all the cases NS responded with a relatively sharp hyperpolarizing response. The first incidence (A) of tension shows that very little force is sufficient to elicit the initial hyperpolarizing response. This trough-like response is likewise observed in later incidences when greater force is applied. Notice that compared to the second tension evocation (B), incidences (C & D) at higher rates of application and increasing amount of force caused hyperpolarizing responses that were sustained in time. The magnified portion of Trial B shows an expanded view of the NS recording. The sharp hyperpolarization develops during the tension change and it peaks close to the tension peak.

To summarize the data obtained in normal saline preparations we plotted the time-integral of the response as a function of the change in tension (Δtension) and as a function of the rate of tension increase, for dorsal and ventral applications. Appendix Figures 7A and 7B show that there was no obvious correlation between the response of NS and these stimulus variables.

Synaptic nature of NS response

The dynamics of the NS response to tension suggests that it is not due to a direct effect of the stimulus on the neuron but a synaptic response evoked by a primary stretch receptor. To distinguish between these two alternatives, we repeated the experiments (n=7) in the presence of high Mg^{2+} solution, a condition that blocks synaptic connectivity in the ganglion.

Appendix Figure 8 shows the response of an NS neuron to tension, studied in normal saline, after 10 min in high Mg^{2+} and after 10 min wash out. In the high Mg^{2+} condition

(Appendix Figure 8B), the NS displayed none of the hyperpolarizing bursts following the initial hyperpolarizing effect induced by tension. However, in several preparations a sustained hyperpolarizing effect, as the one shown in this example, was still observed. The effect of Mg^{2+} was reversed after wash out.

We summarized the data obtained in high Mg^{2+} plotting the time-integral as a function of the difference in tension and the rate of tension application (Appendix Figure 9). Similar to the results for experiments in normal saline, no correlation between the response of NS and the stimulus variables was found in the high Mg^{2+} condition. Moreover, for ventral tension, we observed both positive and negative responses, strongly suggesting that they were probably due to mechanical artifacts, which are more readily caused by ventral tension.

T cell response to body wall tension

Appendix Figure 10 demonstrates the characteristic features of the T cell response to tension stimuli. In the course of tension increase, the T cell fires a series of action potentials. The burst of spikes typically end by the time the tension reaches its maximal level. The firing stops once maximal tension is achieved and remains stable.

Direct (non-synaptic) nature of T response

Additionally we examined the responses of T cells in the presence of high Mg^{2+} to study the properties of the stretch receptor without the added variable of any synaptic input. Appendix Figure 11A presents the various degrees of tension application and magnitude applied on the body wall throughout our recordings. Notice that incident D, in spite of achieving a large tension, did not produce a firing response from the T cell. By comparing the responses in trials A and D,

the results suggest that T cell response may be entirely dependent on the rate of tension increase rather than the magnitude of the tension achieved.

Appendix Figures 11B and C show magnified versions of trial B and C in the same recording. A qualitative observation shows that trial C had a greater amount of force and a faster application rate, as well as an increased firing frequency response. In describing stretch receptor responses to longitudinal muscle displacement, Blackshaw and Thompson (1988) also deduced a two-fold component to T cell electrical response, with a static component dependent on the magnitude of stimuli and a dynamic component dependent on the rate of change in stimuli. Accordingly, the next step in our investigation led us to ask the following: are T cells more sensitive to magnitude or rate of a stretching stimulus?

The data obtained in both normal saline and high Mg^{2+} preparations are summarized in Appendix Figure 12. The instantaneous frequency of T cell response was plotted as a function of the change in tension (Δtension) and the rate of tension speed, for both dorsal and ventral hook placements. Figures 12A and 12C show that there was no obvious correlation between the response of NS and the total tension applied in either of the two experimental conditions. Comparing the individual T cell firing responses to the speed of tension induction demonstrates a high correlation between the two variables for both normal saline and high Mg^{2+} conditions. A correlation was inconclusive for the ventral application due to a limited range of slopes induced in the experiment. Individual cells produce markedly different instantaneous frequencies, but the linearity holds a strong relationship for the recordings within each cell.

re 6. Instantaneous frequency measured as a function of rate of tension application by individual cell. A) ordings from the normal saline condition and the dorsal hook placement. There were no ventral hook eriments done in normal saline. B) Recordings from the high Mg^{2+} condition and both hook placements. There e no observed physiological differences in response between the dorsal and ventral hook placements (see ussion). The plots in a thicker outline were recordings of the ventral hook. Strong linear correlations were erved for both conditions. A linear fit for two cells are not shown in the Mg^{2+} condition due to their limited range.

Discussion- *App*

Relationship of NS and T responses to tension sensitivity

The experiments analyzed whether NS was sensitive to two separate variables: rate of tension increase (slope) and maximal tension attained (max amp). Our results indicate that upon the application of tension NS develops a bursty hyperpolarizing response, but this response failed to show any clear correlation with neither of the two stimulus variables.

The bursty hyperpolarizations were reversibly lost when the recordings were done in high Mg^{2+} solution. These results suggest a chemical relation with the primary tension sensor to the NS. The high Mg^{2+} solution, effectively ceasing synaptic transmissions, seems to have removed any correlation the results suggested in normal saline. As a whole, the results indicate a strictly chemical relationship between the NS and its response to tension sensitivity.

By analyzing the T cell's response to maximal tension and rate of tension increase, we were able to determine the degree of sensitivity the neuron had as a stretch receptor for the two variables. From experiments performed in normal saline and high Mg^{2+}, we have determined that the T cell stretch sensitivity is reserved solely for the rate of tension increase and is not sensitive to the magnitude of tension applied.

Characterization of the low-threshold T response

This brings an interesting observation to the known low-threshold nature of T cell response activation (Nicholls & Baylor, 1968; Blackshaw, 1981). Comparing Appendix Figures 5 and 11 show that all instances of zero firing activity only occurred for low levels of application rate (0.075 mV/s or less) whereas zero firing occurred over a wide range of maximal tension values (0-0.21 V, or 0-0.919 g). In fact, 0.919 g of stretch was the upper limit to a large number

of our recordings. If the rate is not reached, the cell will not fire, no matter the amount of tension (illustrated in Appendix Figure 11A Trial D).

Therefore our results indicate that T cells are speed sensitive rather than tension sensitive, in agreement with previous observations made in the application of pressure rather than tension (Carlton and McVean, 1995).

Differences in normal saline and high Mg^{2+} experimental conditions for T response

Although linear fits for both experimental conditions are highly correlated, these values are exceptional for only those in the high Mg^{2+} solution. In our experiments, there is a wider distribution in the different amounts of tension used to produce T cell responses; however, we did not use a wider distribution of application rates in the normal saline recordings. If our conclusions about the selective T cell sensitivity to tension application rate are true, additional testing with increased range of rates may address this issue.

In relation to the response curve, however, the high Mg^{2+} group demonstrated a higher instantaneous frequency for the same rates of application than in the normal saline group. There are a number of possibilities that could explain this interpretation. The presence of Mg^{2+} could be blocking synaptic information coming into the T cell, thus causing the cell to propagate a stronger signal to our recording devices. However, one T cell in the normal saline exhibited a very similar linear fit to another cell in the high Mg^{2+} condition (NS, m = 121.7; Mg^{2+}, m = 124.1). This could indicate that the differential responses both within and between experimental conditions are accounted for by individual differences in the cell. More experiments under careful control of tension stimuli and with a greater sample size should be performed before reaching a definitive conclusion.

Conclusion- *App*

These results suggest that the NS neuron does not function as a stretch-sensitive mechanoreceptor but seems to receive synaptic input from another source. In the NS-centric network of motor regulation, the NS has continuously been observed to propagate regulation through hyperpolarization of motor neurons (Rodriguez et al., 2009). The vast majority of cases in this study observed a sustained hyperpolarization for the duration in which tension was applied to the body segment. This may be interpreted as the NS exhibiting a regulatory effect on the motor neurons in response to the stimuli received from the stretch-sensing mechanoreceptor and indicates a synaptic relation between their response and the amount of tension induced, but no relation, synaptic nor direct, to the rate of application.

The present study adds to the multifaceted properties of the leech T cell, particularly as a stretch receptor. These results indicate the T cell's collective sensitivity to the velocity of tension. Specifically, the rate of tension application has a substantial correlation with the firing frequency of the T cell. Along with the hyperpolarizing response to tension stimuli (Blackshaw & Thompson, 1988), T cells also directly respond to the speed of induction, as shown by the preparations in the high Mg^{2+} solution. However, no correlations were observed between firing frequency and the amount of force applied onto the body wall.
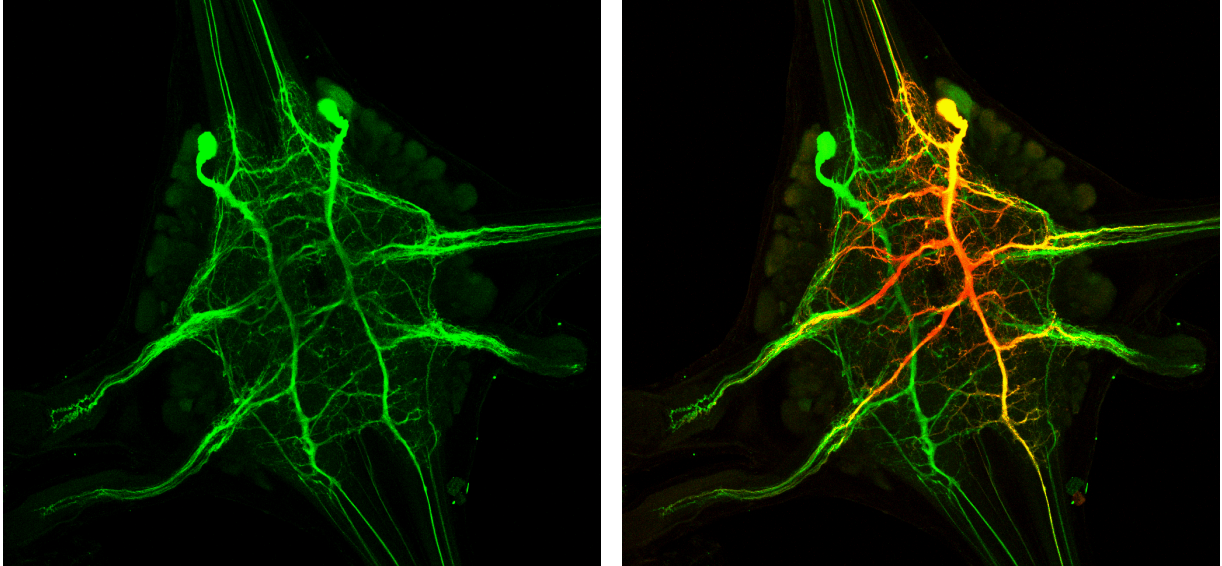
With the current results, one could hypothesize that another cell or group of cells could also exhibit stretch-sensitive properties, particularly to the synaptic relation of tension application rate and the direct relation to magnitude of tension stimuli. With the NS-framework of motor regulation (Wadepuhl, 1989; Rodriguez et al., 2009), there is reason to believe that another neuron or group of neurons are working in tandem with the T cells to communicate

stretch sensitivity through the NS with the overall goal of motor control in response to external stimuli.

More sophisticated machinery and motorized controls would be appropriate for a continued quantitative study into the mechanisms of tension displacement in the NS and T cells. This would account for controls, particularly in basal tension and a steady rate of tension application. Motorized controls would also eliminate the resistance exhibited by the skin once maximal tension is applied, allowing for a more accurate measurement of the sustained tension effect.
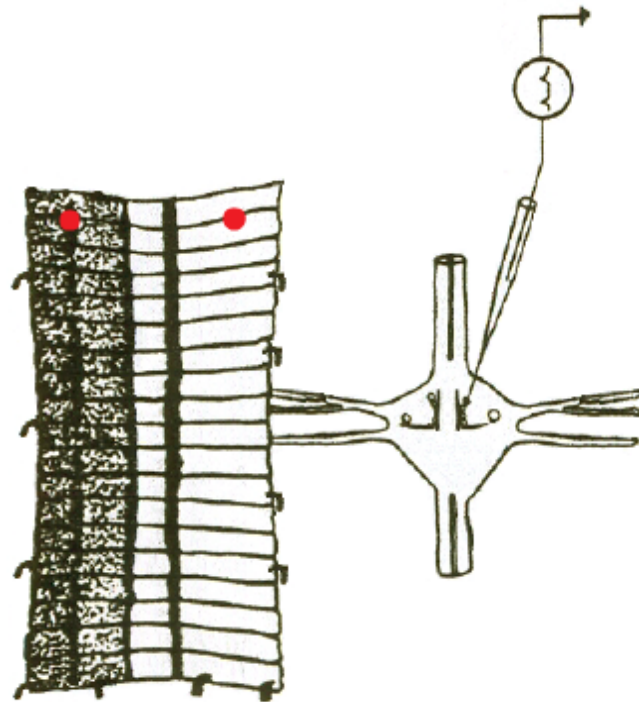
List of Appendix Figures

Appendix Figure 1

Confocal image of a leech mid-body ganglion where the NS neurons were stained with fluorescent dyes. A) Avidin-coupled Alexa reaction to a neurobiotin injection presents the extensive arborization of the NS pair (green fluorescence). B) A red rhodatine dextrane injection into one neuron cannot pass the gap junctions between the two NS cells. Branches in red, orange, and yellow fluorescence indicate the boundaries of one NS cell. (Szczupak Lab)

Appendix Figure 2

Camera lucida image of isolated ganglion and attached body wall. The red areas indicate where

the hook was placed: dorsal, left; ventral, right. (modified from *Mason & Kristan,1982*).

The chart shows a linear plot with y-axis "Tension Measure (V)" ranging from 0 to 0.0025, and x-axis labeled "Weight Applied (g)" ranging from 0 to 12.6 (marks at 0, 2.1, 4.2, 6.3, 8.4, 10.5, 12.6). The fitted line equation is $y = 0.041x + 0.003$ with $R^2 = 0.999$.
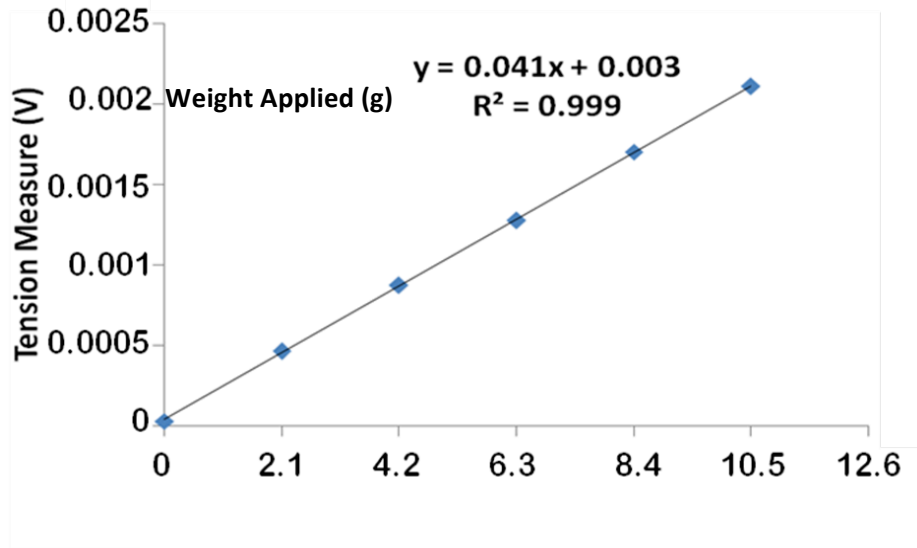
Appendix Figure 3

Test for linearity in tension measurement as a function of weights attached incrementally to the force transducer. Each metal ring weights approximately 2.1g. Tension output is multiplied by a factor of 100 in the ensuing figures.

A

**AE Cell
mV**

0.7 nA   1.7 nA

**Tension
V**

-30

-40

2 sec

B

**P Cell
mV**

0.1

0.09

0.08

*

**Tension
V**

200

0

5 sec

0.06

0.05
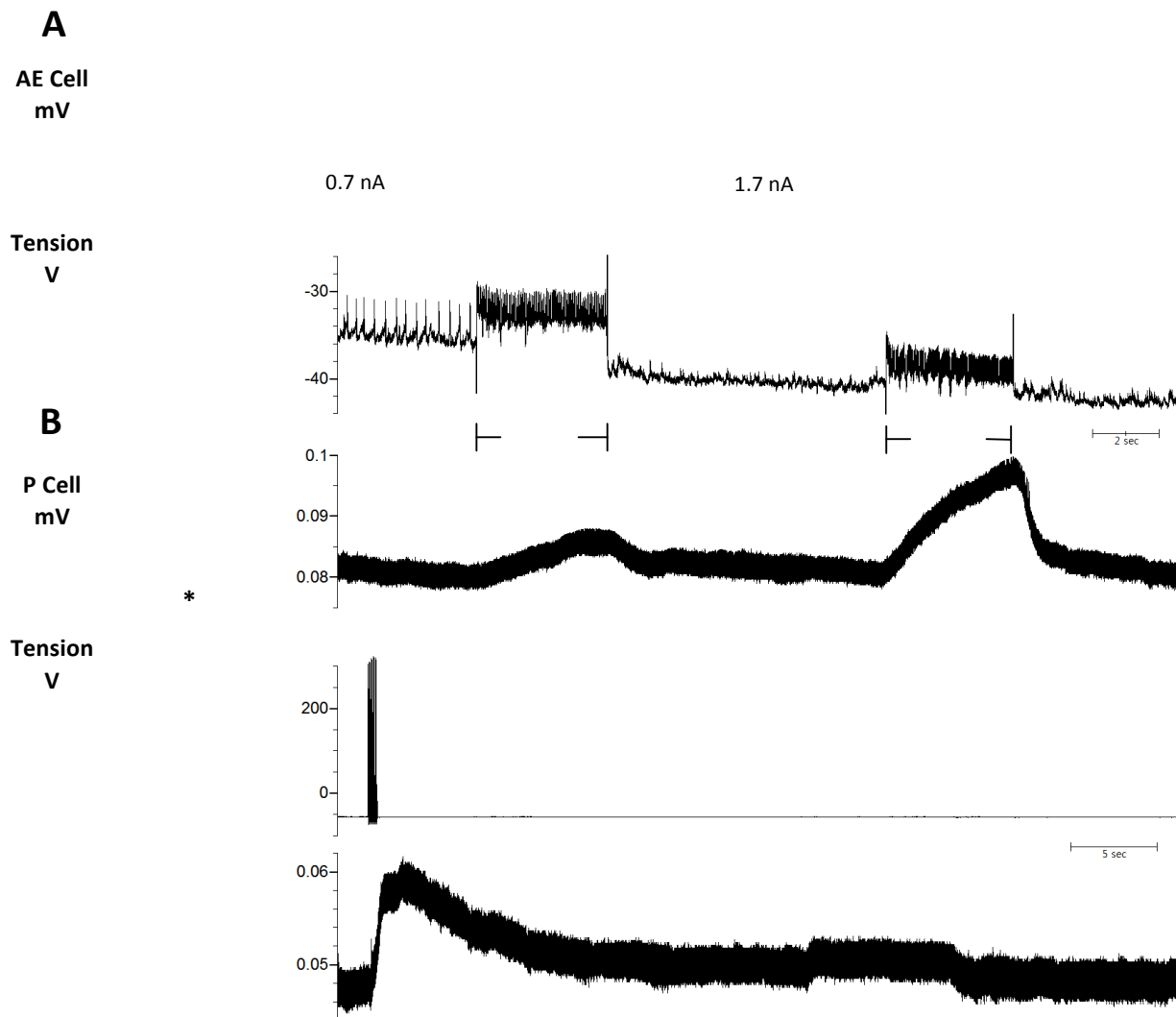
Appendix Figure 4

Control experiments on the effects of tension response from stimulation of A) AE and B) P

neurons. The integrity of the connections from the ganglion to the body wall was confirmed by

stimulating the neurons and testing for a response from the skin.

A) Stimulating the AE produces a direct contraction of the underlying muscle, which causes

contractions in the skin. Increasing the stimulus causes a greater tension response.

B) Stimulation of the P neuron tests the synaptic connections between the P and AE cells. This

verifies full functionality of the relevant connections in the biological preparation.

Notice that the skin returns to baseline tension after a short period without stimulation.
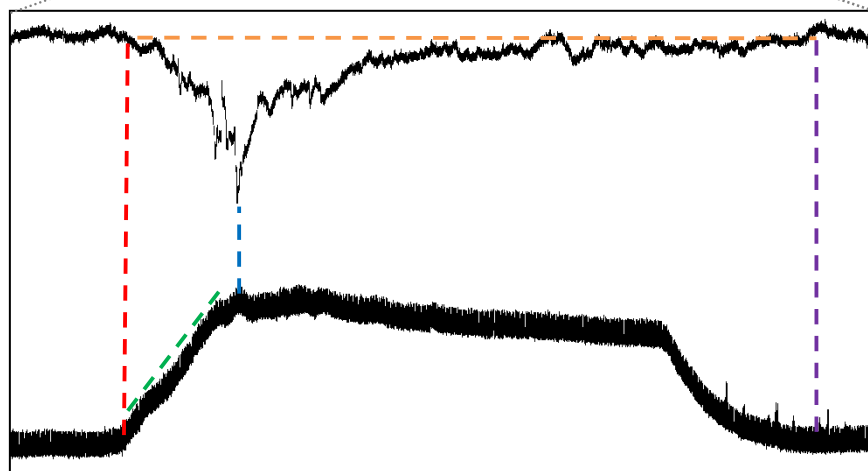
2.2 nA of current stimulation
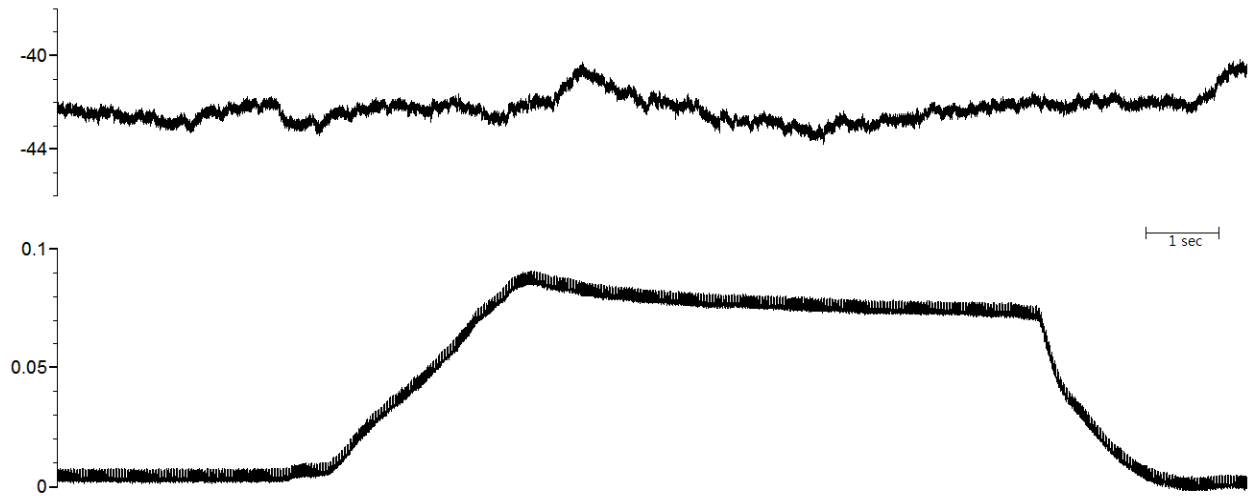
Appendix Figure 5

A T cell with damaged extensions produces no apparent response to a tension stimulus. All other controls, such as the amount of tension applied (Δtension) and the rate of tension speed were kept consistent with those of normal T cell recordings.

Appendix Figure 6

A representative recording of different tension applications to the body segment and corresponding NS response. The vertical red dotted lines indicate the incidences of tension application. Applications varied in amount of force exerted and rate of force increase. Slope (m) is indicated in V/s. Bellow, magnification of Trial B where the different color lines show: start of tension, maximal tension, slope, and baseline Vm_{NS}.

A

B
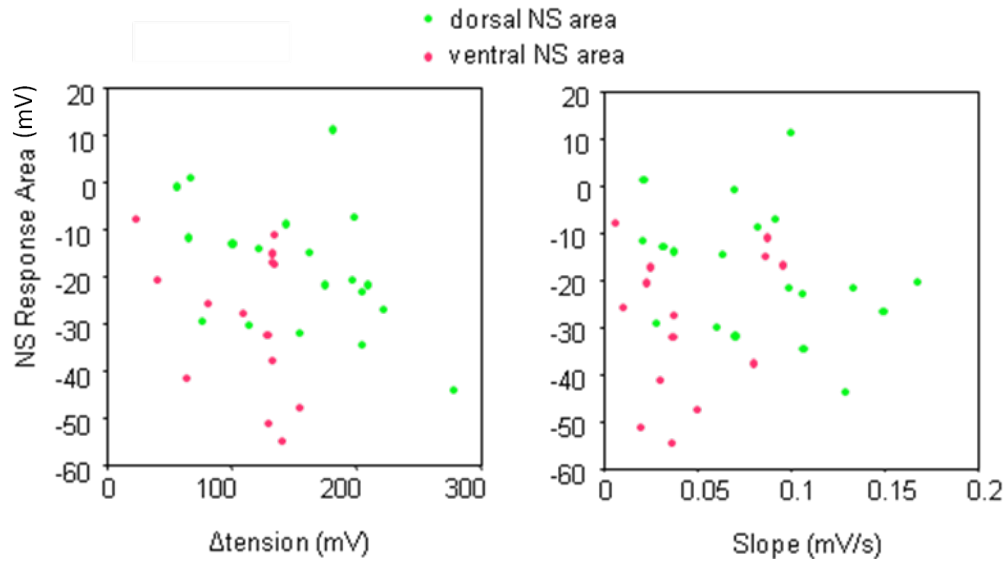
Appendix Figure 7

Response area measured as a function of A) maximum tension (Δtension) and B) slope (rate of tension increase) for experiments in the normal saline condition. No obvious linearity can be drawn for these experiments.
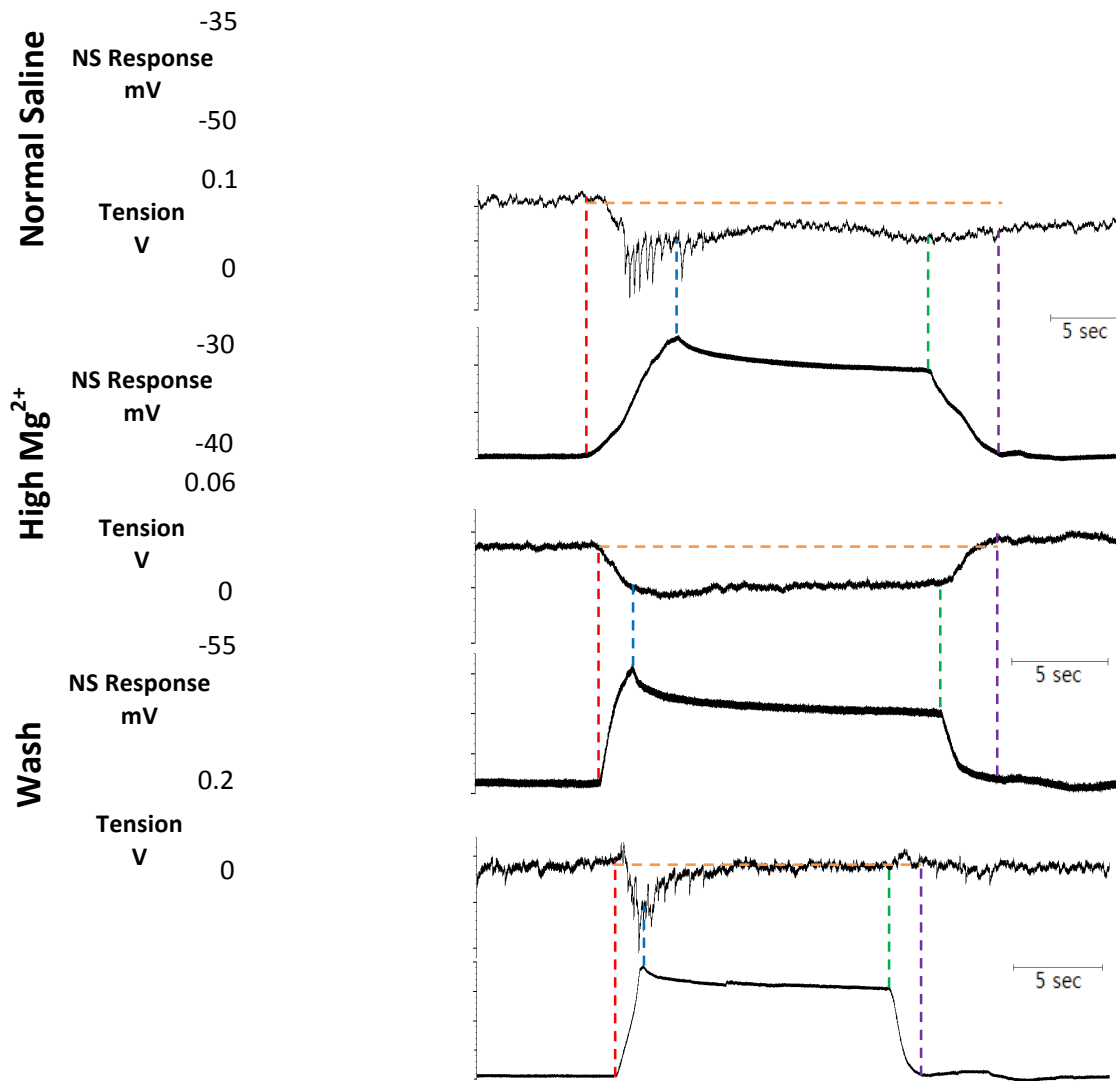
Appendix Figure 8

Differential response in the NS while exposed to the three experimental conditions:

A) Normal Saline. The characteristic response of the NS is a rapid onset of hyperpolarization, followed by bursty hyperpolarizations that are sustained throughout the tension increase.

B) High Mg^{2+}. The bursty response is absent in this experimental condition. The general hyperpolarization remains.

C) Wash. Removal of high Mg^{2+} reverses the cell's response back to the original bursty patterns.

Cursors represent the following approximate values: **start of tension**, **maximal tension**, **end of sustained tension**, **removal of tension**, **baseline Vm_{NS}**.

A

B

NS Response Area (mV)

Appendix Figure 9

Response area measured as a function of A) maximum tension (Δtension) and B) slope (rate of tension increase) for experiments in the high Mg^{2+} condition. No obvious linearity can be drawn for these experiments.
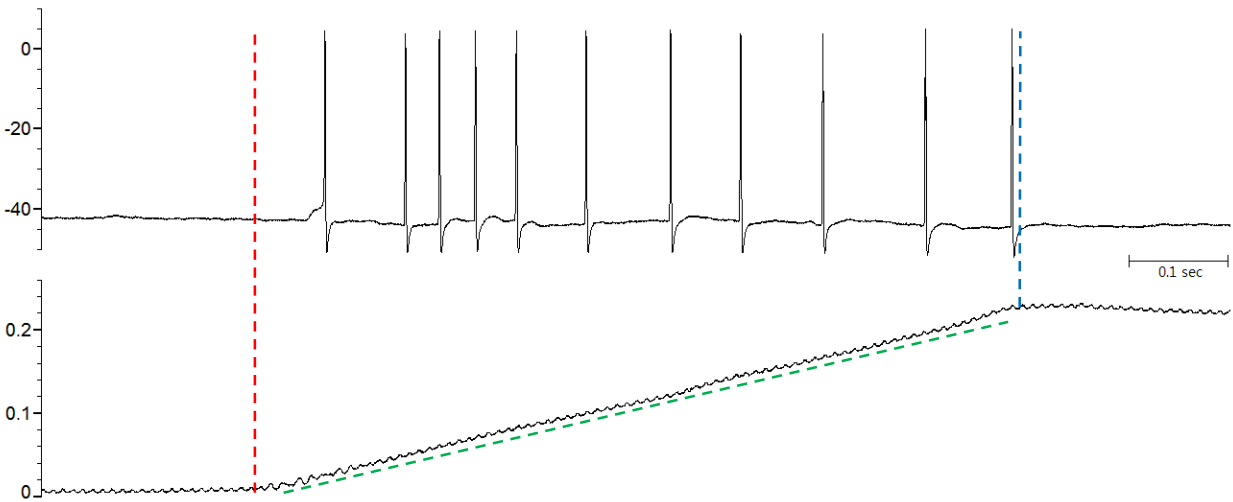
Appendix Figure 10

A typical T cell response to active tension stimulation. This preparation was done in normal

saline. The red and blue dashed lines indicate the start and end of the tension stimulus,

respectively, while the green line presents the approximate slope of the application rate.
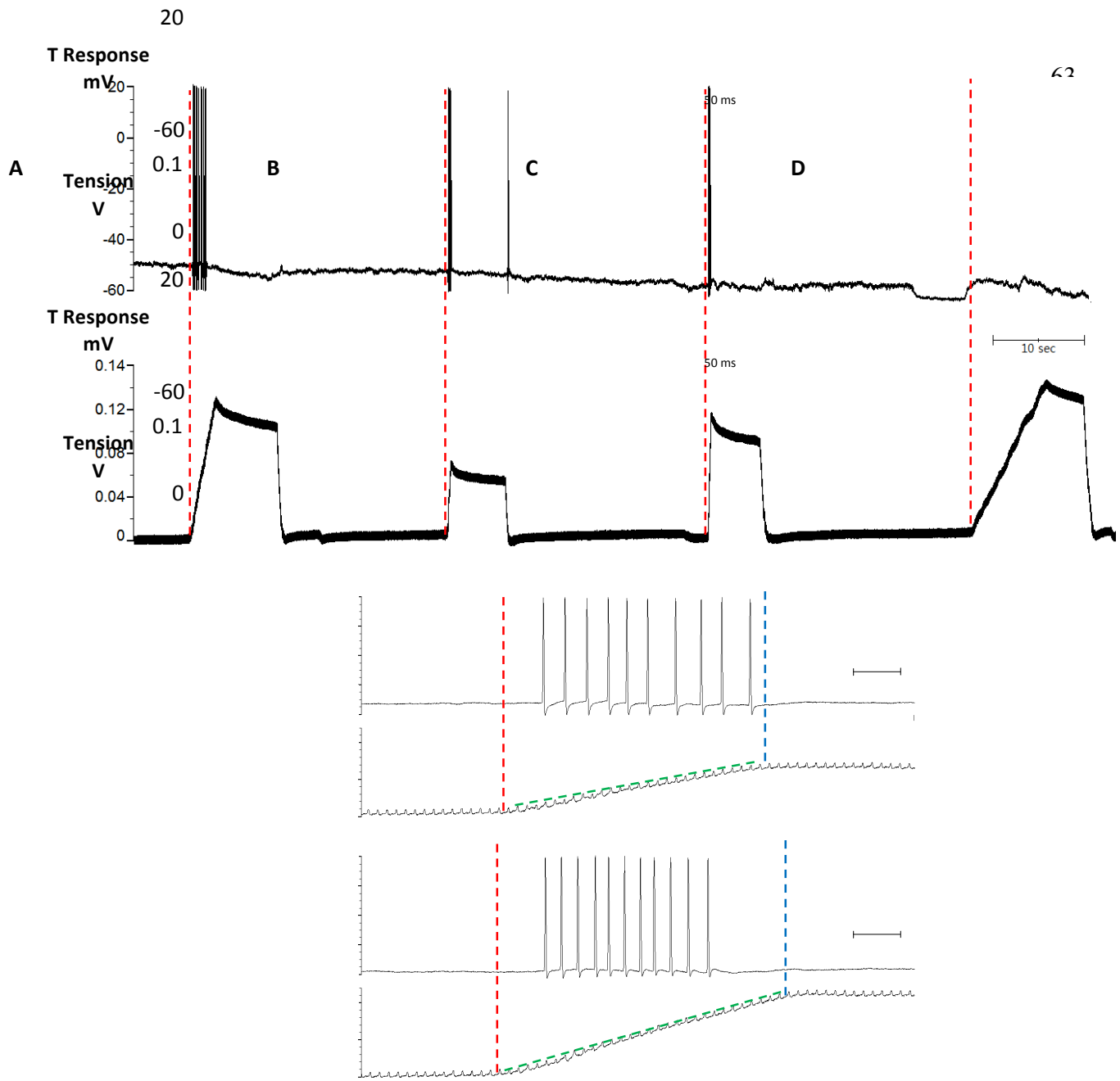
Appendix Figure 11

A representative recording of the responses of T cells to different tension applications to the body segment, in high Mg^{2+}. A) The vertical red dotted lines indicate the incidences of tension application. Measurements varied in amount of force applied and rate of application. B & C) Magnification of Trials B and C, respectively. The red and blue dashed lines indicate the start and end of the tension stimulus, respectively. The green line presents the approximate slope of the tension application.

B

D

Dorsal, normal saline: Instantaneous frequency vs. Total tension

Dorsal & Ventral, high Mg2+: Instantaneous frequency vs. Total tension

Dorsal, normal saline: Instantaneous frequency vs. Rate of application, by cell

$y = 121.7x - 2.705$
$R^2 = 0.923$

$y = 57.15x + 1.600$
$R^2 = 0.862$

Dorsal & Ventral, high Mg^{2+}: Instantaneous frequency vs. Rate of application, by cell

$y = 124.1x + 1.363$
$R^2 = 0.972$

$y = 192.2x - 0.378$
$R^2 = 0.977$

$y = 91.85x + 1.407$
$R^2 = 0.945$

Appendix Figure 12

Instantaneous frequency measured as a function of maximum tension (attained). A&B)

Recordings from the normal saline condition and the dorsal hook placement. There were no

ventral hook experiments done in normal saline. C&D) Recordings from the high Mg^{2+} condition

and both hook placements. Each series of plots represents the responses from an individual cell.

There were no observed physiological differences in response between the dorsal and ventral

hook placements.

References

Arshavsky, Y. I., Deliagina, T. G., Orlovsky, G. N., Panchin, Y. V., Popova, L. B., Sadreyev, R. I. (1998). Analysis of the central pattern generator for swimming in the mollusk. *Ann N Y AcadSci*, 860, 51-69.

Blackshaw, S. E. (1981). Morphology and distribution of touch cell terminals in the skin of the leech. *Journal of Physiology*, 320, 219-228.

Blackshaw, S. E., Nicholls, J. G. (1995). Neurobiology and development of the leech. *Journal of Neurobiology*, 27 (3): 267-276.

Blackshaw, S. E., Nicholls, J. G., Parnas, I. (1982). Physiological responses, receptive fields and terminal arborizations of nocioceptive cells in the leech. *Journal of Physiology*, 326, 251-260.

Blackshaw, S. E., & Thompson, S. W. N. (1988).Hyperpolarizing responses to stretch in sensory neurones innervating the leech body wall muscle. *Journal of Physiology*, 396, 121-137.

Calabrese, R. L., Nadim, F., and Olsen, Ø. H. (1995). Heartbeat control in the medicinal leech: A model for understanding the origin, coordination, and modulation of rhythmic motor patterns. *Journal of Neurobiology*, 27(3): 390-402.

Calabrese, R. L., Norris, B. J., Wenning, A., Wright, T. M. (2011). Coping with variability in small neuronal networks. *Integr Comp Biol*, 2011 Dec; 51(6): 845-55.

Carlton, T., McVean, A. (1995).The role of touch, pressure, and nociceptive mechanoreceptors of the leech in unrestrained behavior. *Journal of Comparative Physiology*, 177: 781-791.

Goaillard, J. M., Taylor, A. L., Schulz, D. J., Marder, E. (2009).Functional consequences of animal-to-animal variation in circuit parameters. *Nat Neurosci*, 12(11): 1424-30.

Katz, B. & Miledi, R. (1963).A study of spontaneous miniature potentials in spinal motoneurones. *Journal of Physiology*, 168, 309-422.

Jellies, J. & and Kueh, D. (2012).Centrally patterned rhythmic activity integrated by a peripheral circuit linking multiple oscillators. *J Comp Physiol A*, 198(8):567-82

Kristan, W., Calabrese, R., & Friesen, W. (2005).Neuronal control of leech behavior. *Progress in Neurobiology*, 76(5), 279-327.

Laverack, M. S. (1969).Mechanoreceptors, photoreceptors and rapid conduction pathways in the leech, Hirudo medicinalis. *Journal of Experimental Biology*, *50*, 129-140.

Norris, B. J., Wenning A., Wright, T.M., Calabrese, R. L. (2011). Constancy and variability in the output of a central pattern generator. *Journal of Neuroscience*, 31 (12): 4463-4674

Nicholls, J. G., & Baylor, D. A. (1968).Specific modalities and receptive fields of sensory neurons in CNS of the leech. *Journal of Neurophysiology*, 31(5), 740-56.

Maranto, A. R., Calabrese, R. L. (1984). Neural control of the hearts in the leech, Hirudo medicinalis. *J Comp Physiol A*, 154: 367-380.

Mason, A., &Kristan, W. (1982).Neuronal excitation, inhibition, and modulation of leech longitudinal muscle. *Journal of Comparative Physiology A*, 146, 527-36.

Prinz, A. A., Thirumalai, V., Marder, E. (2003). The functional consequences of changes in the strength and duration of synaptic inputs to oscillatory neurons. *J Neurosci*, 23, 943-954.

Rela, L., &Szczupak, L. (2006).In situ characterization of a rectifying electrical junction. *Journal of Neurophysiology*, *97*(2), 1405-1412.

Rela, L., &Szczupak, L. (2003). Coactivation of motoneurons regulated by a network combining electrical and chemical synapses. *Journal of Neuroscience*, *23*(2), 682-692.

Rela, L., Yang, S. M., &Szczupak, L. (2009). Calcium spikes in a leech nonspiking neuron. *Journal of Comparative Physiology A*, *195*(2), 139-150.

Rodriguez, M. J., Alvarez, R. J., &Szczupak, L. (2012).Effect of a nonspiking neuron on motor patterns of the leech. *Journal of Neurophysiology*, 107, 1917-1924.

Rodriguez, M. J., Perez-Etchegoyen, C. B., &Szczupak, L. (2009). Premotor nonspiking neurons regulate coupling among motoneurons that innervate overlapping muscle fiber population. *Journal of Comparative Physiology A*, 195(5), 491-500.

Thompson, W. J. and Stent, G. S. (1976a).Neuronal control of heartbeat in the medicinal leech I. Generation of the vascular constriction rhythm by heart motor neurons. *J. Comp. Physiol*, 111: 261-279

Tresch, M. C., Saltiel, P., dÁvella A., Bizzi, E. (2002)Coordination and localization inspinal motor systems. *Brain Research Rev*, 40: 66–79, 2002.

Wadepuhl, M. (1989).Depression of excitatory motoneurones by a single neurone in the leech central nervous system. *Journal of Experimental Biology*, *143*, 509-527.

Wenning, A., Cymbalyuk, G. S., Calabrese, R. L. (2004). Heartbeat control in leeches. I. Constriction pattern and neural modulation of blood pressure in intact animals. *J Neurophysiol*, 91: 382–396.

Wenning, A., Hill, A. A., Calabrese, R. L. (2003). Heartbeat control in leeches. II. Fictive motor pattern. *J Neurophysiol*, 91(1): 397-409.

Wenning, A.& Meyer, E. P. (2007). Hemodynamics in the leech: blood flow in two hearts switching between two constriction patterns. *J Exp Biol*, 2007 Aug; 210 (Pt 15): 2627-36

Wenning, A., Norris, B.J., Doloc-Mihu, A., and Calabrese, R. L. (2011).Bringing up the rear: New premotor interneurons add regional complexity to a segmentally distributed motor pattern*. J Neurophysiol*. 106: 2201-2215

Wenning, A., Norris, B.J., Doloc-Mihu, A., and Calabrese, R. L. (2014).Variation in motor

output and motor performance in a centrally generated motor pattern. *Manuscript accepted*

for publication.